SINGULARITY FORMATION IN THE DETERMINISTIC AND STOCHASTIC FRACTIONAL BURGERS EQUATIONS

SINGULARITY FORMATION IN THE DETERMINISTIC AND STOCHASTIC FRACTIONAL BURGERS EQUATIONS

By ELKIN WBEIMAR RAMÍREZ, M.Sc

A Thesis Submitted to the School of Graduate Studies in Partial Fulfilment of the Requirements for the Degree Master of Science

McMaster University MASTER OF SCIENCE (2020)

Hamilton, Ontario (Mathematics)

TITLE: SINGULARITY FORMATION IN THE DETERMINISTIC AND STOCHAS-

TIC FRACTIONAL BURGERS EQUATIONS

AUTHOR: Elkin Wbeimar Ramírez, M.Sc (CIMAT)

SUPERVISOR: Professor Bartosz Protas

NUMBER OF PAGES: iv, 66

Abstract

Motivated by the results concerning the regularity of solutions to the fractional Navier-Stokes system and questions about the influence of noise on the formation of singularities in hydrodynamic models, we have explored these two problems in the context of the fractional 1D Burgers equation. First, we performed highly accurate numerical computations to characterize the dependence of the blow-up time on the the fractional dissipation exponent in the supercritical regime. The problem was solved numerically using a pseudospectral method where integration in time was performed using a hybrid method combining the Crank-Nicolson and a three-step Runge-Kutta techniques. A highlight of this approach is automated resolution refinement. The blow-up time was estimated based on the time evolution of the enstrophy (H^1 seminorm) and the width of the analyticity strip. The consistency of the obtained blow-up times was verified in the limiting cases. In the second part of the thesis we considered the fractional Burgers equation in the presence of suitably colored additive noise. This problem was solved using a stochastic Runge-Kutta method where the stochastic effects were approximated using a Monte-Carlo method. Statistic analysis of ensembles of stochastic solutions obtained for different noise magnitudes indicates that as the noise amplitude increases the distribution of blow-up times becomes non-Gaussian. In particular, while for increasing noise levels the mean blow-up time is reduced as compared to the deterministic case, solutions with increased existence time also become more likely.

Acknowledgements

I would like to express my gratitude to my supervisor Dr. Bartosz Protas for his valuable advice, comments and remarks thought the learning process of this thesis. Likewise, I would like to thank Dr. Dmitry Pelinovsky and Dr. Nicholas Kevlahan for their comments on the thesis. Also, I would like to thank McMaster University for giving me the opportunity of an academic and cultural interchange. Last but not least, I would like to thank my loved ones and friends, who have supported me throughout this entire process.

Contents

List of Figures

List of Tables

Chapter 1

Introduction

Fluid dynamics is an active area of research in mathematics centered around a few key models. The first step in their study is usually to verify their local and global well-posedness which is often quite challenging. Arguably, the most famous problem in fluid dynamics is concerning the three-dimensional Navier-Stokes Equations (NSE),

$$\left(\frac{\partial}{\partial t} - \nu \boldsymbol{\nabla}^2\right) \mathbf{u}(\mathbf{x}, t) = -\boldsymbol{\nabla} p(\mathbf{x}, t) - \mathbf{u}(\mathbf{x}, t) \cdot \nabla \mathbf{u}(\mathbf{x}, t) \qquad \mathbf{x} \in \Omega, \ t > 0, \quad (1.1a)$$

$$\boldsymbol{\nabla} \cdot \mathbf{u}(\mathbf{x}, t) = 0 \qquad\qquad\qquad \mathbf{x} \in \Omega, \ t > 0, \quad (1.1b)$$

$$\mathbf{u}(\mathbf{x}, 0) = \mathbf{g}(\mathbf{x}) \qquad\qquad\qquad \mathbf{x} \in \Omega, \ t = 0, \quad (1.1c)$$

where Ω is a three-dimensional physical domain, $\mathbf{u}$ and p are the velocity vector field and the scalar pressure field. Equations (1.1a) and (1.1b) represent, respectively, the conservation of momentum and mass, whereas $\mathbf{g}$ is the initial condition. In addition, $\mathbf{u}$ is subject to periodic boundary conditions in Ω. This is one of the Millennium

Problems formulated by the Clay Mathematics Institute [Fef00]. For a given smooth initial data, the problem is to either prove global existence and smoothness of the solution or formation of a singularity at a finite time. Since the Navier-Stokes (NS) system is used in many applications ranging from the study of blood flow to the design of aircrafts, the present situation where the well-posedness of this model remains open question is highly unsatisfactory. A classical approach to study existence of solutions relies on "energy methods", where one seeks to derive a priori bounds on the norms of the solution in certain function spaces [Doe09]. Some of these norms correspond to physically important quantities such as enstrophy. A "blow-up" occurs when a solution norm becomes infinite in finite time.

Since the main problem is so challenging, many interesting insights have been obtained studying its various modifications or simplifications. One common simplification is to consider problems defined on periodic or unbounded domains, rather than domains with solid boundaries. For instance, in [KP02], it was proved that the NSE is globally well-posed in the classical sense with dissipation $(-\boldsymbol{\Delta})^{\alpha}$ and $\alpha \geq 5/4$ (see expression (2.2) for the definition of the fractional Laplacian). The standard dissipative term in the NSE is $\boldsymbol{\Delta}$, but in this example, it was replaced by the fractional Laplacian and that nice result was obtained. A common simplification of the NSE is obtained by restricting it to one dimension and dropping the incompressibility condition. As a result, one obtains the one-dimensional Burgers equation which together with its inviscid variant have received a lot of attention and have been shown to possess many interesting properties [KL04]. Motivated by the aforementioned result about the global well-posedness of the three-dimensional fractional

NS system, a fractional version of the one-dimensional Burgers equation was considered in [KNS08, YP18]. It is an interesting model, because depending on the value of the fractional dissipation exponent, one obtains global well-posedness of solution, or finite-time blow up (more of this in Chapter 2). The first goal of this thesis is to characterize this behavior quantitatively by performing very accurate numerical computations.

Another emerging research direction concerns the effect of stochastic excitations on the behavior of hydrodynamic models and the recent progress in this field is reviewed in the monograph [DDFR12]. Among several questions presented in that work, the one that motivates our study concerns the possibility whether suitable random perturbations can prevent the emergence of singularities. Thus, the second objective of this thesis is to prove this hypothesis computationally in the context of the fractional Burgers equation. We emphasize that both objectives of this thesis represent original research contributions.

In order to achieve our research goals, in Chapter 2, we set our cases of study, the deterministic and the stochastic fractional Burgers equation, recalling some known results and defining two key quantities, important for characterizing the process of singularity formation. Next, in Chapter 3 we will introduce the numerical methods that we used to solve both the deterministic and the stochastic fractional Burgers equation. In this chapter we will also discuss how we are going to compute the estimates for the blow-up time. Then, in Chapter 4 we will present the obtained numerical results. Lastly, in chapter 5 we will give a summary of the main results and future work. At the end, we include appendices with some details about the

choice of the noise and one limiting case for a certain parameter.

Chapter 2

Fractional Burgers Equation

In this chapter we are going to present two versions of the fractional Burgers equation, the deterministic and the stochastic representation. We will also present two key quantities in our study of the regularity of the solution of these systems, the enstrophy and the width of the analyticity strip.

2.1   Deterministic version

Consider the 1D fractional Burgers equation

$$\partial_t u + \frac{1}{2}\, \partial_x u^2 + \nu \, (-\Delta)^\alpha u = 0 \quad \text{in } (0, T] \times (0, 2\pi), \tag{2.1a}$$

$$u(t, 0) = u(t, 2\pi) \quad \text{for } t \in (0, T], \tag{2.1b}$$

$$\partial_x u(t, 0) = \partial_x u(t, 2\pi) \quad \text{for } t \in (0, T], \tag{2.1c}$$

$$u(0, x) = g(x) \quad \text{for } x \in (0, 2\pi), \tag{2.1d}$$

where $\nu > 0$ is the viscosity coefficient, $\alpha \in [0, 1]$ is the fractional dissipation exponent and $(-\Delta)^\alpha$ is the fractional Laplacian. For an adequately smooth function $v(x)$, the fractional Laplacian is defined as

$$\mathcal{F}\left[(-\Delta)^\alpha v\right](k) = |k|^{2\alpha} \mathcal{F}\left[v\right](k) = |k|^{2\alpha} \widehat{v}_k, \tag{2.2}$$

where $\mathcal{F}\left[\cdot\right](k)$ refers to Fourier coefficients with wavenumber $k \in \mathbb{Z}$. They are denoted as $\mathcal{F}\left[v\right](k) = \widehat{v}_k$. Also, $T > 0$ represents the length of the time window and $g \in H_p^1(0, 2\pi)$ is the initial condition, where $H_p^1(0, 2\pi)$ is the Sobolev space of square-integrable periodic functions on $(0, 2\pi)$ such that their first derivatives are also square-integrable. The norm on $H_p^1(0, 2\pi)$ is

$$\begin{aligned}
||v(\cdot)||^2_{H_p^1(0,2\pi)} &= ||v(\cdot)||^2_{L_p^2(0,2\pi)} + ||\nabla v(\cdot)||^2_{L_p^2(0,2\pi)} \\
&= \sum_{k=-\infty}^{\infty} \left(1 + |k|^2\right) |\widehat{v}_k|^2,
\end{aligned} \tag{2.3}$$

where $L_p^2(0, 2\pi)$ stands for the space of square-integrable 2π-periodic functions. The last equality in expression (2.3) is obtained by Parseval's identity. We will also use the space $H_p^s(0, 2\pi)$, which is

$$H_p^s(0, 2\pi) = \left\{ v \in L_p^2(0, 2\pi) : \sum_{k=-\infty}^{\infty} \left(1 + |k|^2\right)^s |\widehat{v}_k|^2 < \infty \right\}, \quad s > 0. \tag{2.4}$$

Some of known results that address questions regarding existence and uniqueness of solutions of system (2.1) are found in [KNS08] and are summarized below.

Theorem 2.1 (subcritical case). *Assume that $\alpha > 1/2$, and the initial data $g \in H^s$,*

$s > 3/2 - 2\alpha$, $s \geq 0$. *Then there exists a unique global solution of the problem* (2.1) *that belongs to* $C([0, \infty), H^s)$ *and is real analytic in x for $t > 0$.*

Theorem 2.2 (critical case). *Assume that $\alpha = 1/2$, and $g \in H^s$, $s > 1/2$. Then there exists a global solution of the system* (2.1) *which is real analytic in x for any $t > 0$.*

If $1/2 \leq \alpha \leq 1$, then $-1/2 \leq 3/2 - 2\alpha \leq 1/2$. Therefore, problem (2.1) is globally well-posed for an initial condition g in $H_p^1(0, 2\pi)$ by Theorems 2.1 and 2.2.

Theorem 2.3 (supercritical case). *Assume that $0 < \alpha < 1/2$. Then there exists smooth periodic initial data g such that the solution u of* (2.1) *blows up in H^s for each $s > \frac{3}{2} - 2\alpha$ in a finite time.*

Solutions of the system (2.1) in the supercritical regime are analytic until right before they blow up. Under the assumption that $g \in H_p^1(0, 2\pi)$, solutions of system (2.1) will blow up for some initial data when $1/4 < \alpha < 1/2$ by Theorem 2.3 (see figure 2.1). For $\alpha \in [0, 1/4]$, the picture appears more nuanced for several reasons. First of all, if $0 < \alpha \leq 1/4$ and $g \in H_p^1(0, 2\pi)$, Theorem 2.3 concludes nothing. Secondly, we found numerical evidence that solutions of system (2.1) still blow up for values of α in $(0, 1/4)$ and a specific initial condition $g \in H_p^1(0, 2\pi)$. Lastly, the authors in [YP18] proposed a conjecture which states that if $0 \leq \alpha \leq 1/4$, system (2.1) is not even locally well-posed in H_p^1 for some initial data. Therefore, it may appear that the condition $s > \frac{3}{2} - 2\alpha$ in Theorem 2.3 is not sharp, in the sense that blow-up may also occur outside that condition under certain initial data. For instance, when $s = 1$, $0 < \alpha \leq \frac{1}{4}$ and $g(x) = \sin(x)$.
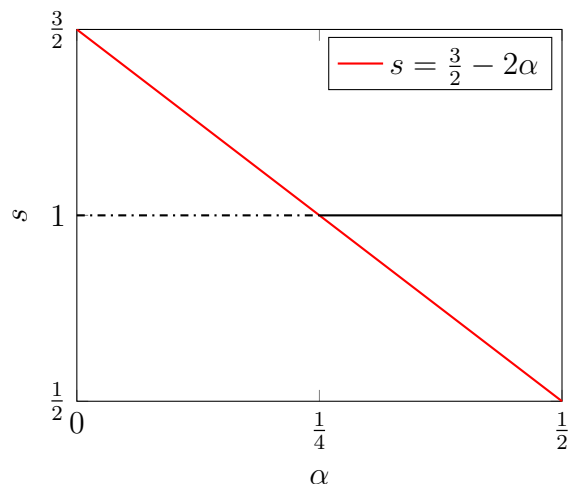
Figure 2.1: Borderline relation between s and α in Theorem 2.3. For a given value of α in system (2.1), blow-up occurs for initial data in $H^s_p(0, 2\pi)$ with values of s above the red line. The black horizontal line represents H^1, which is the case we are interested in here.

2.1.1 Limiting cases

Some of the limiting cases that we also consider in this thesis are $\nu = 0$ and $\alpha = 0$. For $\nu = 0$, system (2.1) becomes the inviscid Burgers system (2.5) regardless the value of the fractional dissipation exponent α

$$\partial_t u + \frac{1}{2} \partial_x u^2 = 0 \quad \text{in } (0, T) \times (0, 2\pi), \tag{2.5a}$$

$$u(t, 0) = u(t, 2\pi) \quad \text{for } t \in (0, T], \tag{2.5b}$$

$$u(0, x) = g(x) \quad \text{for } x \in (0, 2\pi), \tag{2.5c}$$

where T and g are as in system (2.1). This system represents a well-known and well-understood example for the formation of shocks [KL04]. For some initial conditions, solutions develop sharp fronts resulting in blow-up at a finite time in $H_p^1(0, 2\pi)$. That finite time can be computed as

$$T^* = \begin{cases} \infty & \text{if } g'(x) \geq 0 \text{ for all } x \in [0, 2\pi], \\ -\frac{1}{\inf g'(x)} & \text{otherwise.} \end{cases} \tag{2.6}$$

Now, considering $\alpha = 0$, the fractional Laplacian $(-\Delta)^\alpha$ in equation (2.1a) becomes the identity operator. So the system (2.1) turns into

$$\partial_t u + \frac{1}{2} \partial_x u^2 + \nu\, u = 0 \quad \text{in } (0, T) \times (0, 2\pi), \tag{2.7a}$$

$$u(t, 0) = u(t, 2\pi) \quad \text{for } t \in (0, T], \tag{2.7b}$$

$$u(0, x) = g(x) \quad \text{for } x \in (0, 2\pi). \tag{2.7c}$$

The solution of this equation can be found in Appendix A. The expression for the blow-up time is given by

$$T^* = \begin{cases} \infty & \text{if } g'(x) + \nu \geq 0 \text{ for all } x \in [0, 2\pi], \\ -\frac{1}{\nu} \ln\left(\frac{\nu}{\inf g'(x)} + 1\right) & \text{otherwise.} \end{cases} \tag{2.8}$$

2.2   Stochastic version

The second case of study in this thesis is the stochastic version of the system (2.1). In principle, stochastic forcing can be additive or multiplicative. It is known that

multiplicative noise has an analogous effect to dissipative terms in problems of fluid dynamics [DDFR12]. Therefore, if we consider this type of noise, no major changes in the solution of system (2.1) are expected, since the dissipative term is already present. So only additive noise will be considered and the stochastic fractional Burgers equation that we are going to consider is given by

$$\partial_t u + \frac{1}{2}\,\partial_x u^2 + \nu\,(-\Delta)^\alpha u = \zeta(t,x) \quad \text{in } (0,T] \times (0,2\pi), \tag{2.9a}$$

$$u(t,0) = u(t,2\pi) \quad \text{for } t \in (0,T], \tag{2.9b}$$

$$\partial_x u(t,0) = \partial_x u(t,2\pi) \quad \text{for } t \in (0,T], \tag{2.9c}$$

$$u(0,x) = g(x) \quad \text{for } x \in (0,2\pi), \tag{2.9d}$$

where $\zeta(t,x)$ is an additive stochastic forcing, and ν, T, $(-\Delta)^\alpha$ and g are as in system (2.1). Now, the solution $u(\omega;t,x)$ of system (2.9) at any given point $(t,x) \in (0,T] \times (0,2\pi)$ and $\omega \in \Omega$, where Ω is some probability space, becomes a random variable . We will refer to ζ as the noise of the system (2.9).

It is common to use a Gaussian noise as a stochastic forcing. However, as shown in Appendix B, in such case solutions of system (2.9) do not remain in $H^1_p(0,2\pi)$ even in the subcritical case. Hence, following the earlier study in [PP18], we will consider a colored-in-space Gaussian noise

$$\zeta(t,x) = \sigma\frac{dW(t)}{dt}, \tag{2.10}$$

where $\sigma > 0$ is a constant and $W(t)$ is a cylindrical Wiener process given by the

expression

$$W(t) = \sum_{j \in \mathbb{N}} \gamma_j \, \beta_j(t) \, \chi_j, \tag{2.11}$$

where $\{\beta_j(t)\}_{j \in \mathbb{N}}$ are an independent and identically distributed (i.i.d.) standard Brownian motions, $\{\chi_j\}_{j \in \mathbb{N}}$ are a trigonometric orthonormal basis of $L_p^2(0, 2\pi)$ and $\{\gamma_j\}_{j \in \mathbb{N}}$ are scaling coefficients. We will set $\chi_0 = 1$, $\chi_{2j} = \sqrt{2} \cos(jx)$ and $\chi_{2j-1} = \sqrt{2} \sin(jx)$ and

$$\gamma_0 = 0, \quad \gamma_{2k-1} = \gamma_{2k} = \frac{1}{k}, \quad k > 0. \tag{2.12}$$

The reasons of the choice of γ_j and χ_j are also explained in Appendix B.

The relevant concept of solution in this case is not a classical one because of the non regularity of the Weiner process. Therefore, we will be using the concept of *mild solution* [LPS14]. Before defining it, we need to rewrite system (2.9) as

$$du = \left(-\frac{1}{2} \partial_x u^2 - \nu \, (-\Delta)^\alpha u \right) dt + \sigma \, dW \quad \text{in } (0, T] \times (0, 2\pi), \tag{2.13a}$$

$$u(t, 0) = u(t, 2\pi) \quad \text{for } t \in (0, T], \tag{2.13b}$$

$$\partial_x u(t, 0) = \partial_x u(t, 2\pi) \quad \text{for } t \in (0, T], \tag{2.13c}$$

$$u(0, x) = g(x) \quad \text{for } x \in (0, 2\pi). \tag{2.13d}$$

We can then define a mild solution of system (2.13) as

$$u(t) = e^{-tA} g - \frac{1}{2} \int_0^t e^{-(t-s)A} \partial_x u^2 ds + \sigma \int_0^t e^{-(t-s)A} dW(s), \tag{2.14}$$

11

where $g(x)$ is the initial condition (2.13d), $A = \nu\,(-\Delta)^{\alpha}$, the semigroup e^{-tA} is defined in terms of its action on the elements of the basis $\{\phi_k\}_{k\in\mathbb{Z}} = \{e^{ikx}\}_{k\in\mathbb{Z}}$ of $L_p^2(0, 2\pi)$ as $e^{-tA}e^{ikx} = e^{-\nu t|k|^{2\alpha}}e^{ikx}$ and the second integral is understood in Itô's sense.

2.3   Diagnostic quantities

We will be investigating two quantities that will help us to understand behaviours of solutions of systems (2.1) and (2.9), in particular, whether or not these solutions blow up. These quantities are the enstrophy and the width of the analyticity strip.

Firstly, *The enstrophy* is defined as the seminorm:

$$\mathcal{E}(t) = \pi \int_0^{2\pi} |\partial_x u(t, x)|^2 \; dx. \tag{2.15}$$

Since shock formation implies the enstrophy becomes infinitive, the boundedness of this quantity is an indication of the regularity of the solution. We note that the regularity criterion is also valid for the 3D Navier-Stokes system [FT89].

Secondly, *the width of the analyticity strip* at a time t, $\delta(t)$, is defined as the distance of the nearest complex singularity to the real domain of the solution at the time t. To understand the importance of this quantity, let us state the following theorem from [Tre00]

Theorem 2.4. *Let* $u \in L^2(\mathbb{R})$ *have Fourier Transform* $\widehat{u}$. *If there exists* $a, c > 0$, *such that* u *can be extended to an analytic function in the complex strip* $|\Im(z)| < a$ *with* $||u(\cdot + iy)|| \leq c$ *uniformly for all* $y \in (-a, a)$, *where* $||u(\cdot + iy)|| \leq c$ *is the* L^2

norm along the horizontal line $\Im(z) = y$, then $u_a \in L^2(\mathbb{R})$, where $u_a(k) = e^{a|k|}\widehat{u}(k)$, $k \in \mathbb{R}$. The converse also holds.

This theorem also applies to functions defined on periodic domains. The largest value of a in Theorem 2.4 is exactly the width of the analyticity strip of $u(t, x)$. In the context of problem (2.1), a solution ceases to be analytic when the singularities present in its extension into the complex plane collapse into the x-axis, in which case the width of the analyticity strip $\delta(t)$ vanishes. In other words, the solution blows up. Since solutions of the stochastic system (2.9) are not, in general, analytic in x, the width of the analyticity strip cannot be used to characterized their regularity.

Chapter 3

Numerical Approaches

3.1 Deterministic Fractional Burgers Equation

For solving system (2.1) numerically, we used the Fourier-Galerkin pseudo-spectral approach due to the periodicity of the boundary conditions. So let us assume that the solution can be approximated as

$$u_N(t,x) = \sum_{k=-N/2+1}^{N/2} \widehat{u}_k(t)e^{ikx}, \tag{3.1}$$

where $\widehat{u}_k(t)$ are the Fourier coefficients of $u(t,x)$ given by

$$\widehat{u}_k(t) = \frac{1}{2\pi} \int_0^{2\pi} u(t,x)\, e^{-ikx} dx, \tag{3.2}$$

and $N = 2^n$, for some $n \in \mathbb{N}$, is the number of Fourier modes that we are going to use to approximate the solution. Notice that even though we are using N Fourier

modes, it is only necessary to compute half of them, since solutions of system (2.1) are real-valued functions. It means that the conjugate symmetry property holds and the Fourier coefficients satisfy $\widehat{u}_{-k} = \overline{\widehat{u}_k}$, $k = -N/2, ..., N/2$ and the bar denotes complex conjugate. Also, $\widehat{u}_0(t) = 0$ for all t, because we chose to work with initial data with zero mean and the mean is preserved by the system evolution. Now, plugging (3.1) in (2.1) leads us to the system of ordinary differential equations (ODE),

$$\frac{d\widehat{\mathbf{u}}(t)}{dt} = \mathbf{r}(\widehat{\mathbf{u}}(t)) + \mathbf{A}\widehat{\mathbf{u}}(t), \tag{3.3a}$$

$$\widehat{\mathbf{u}}(0) = \widehat{\mathbf{g}}, \tag{3.3b}$$

where $\widehat{\mathbf{u}}(t) = \left[\widehat{u}_1(t), \widehat{u}_2(t), ..., \widehat{u}_{N/2}(t)\right]^T$ and $\widehat{\mathbf{g}} = \left[\widehat{g}_1, \widehat{g}_2, ...\widehat{g}_{N/2}\right]^T$ are the vectors of Fourier coefficients of the solution at the time t and the initial condition $g(x)$, respectively. The symbol $\mathbf{r}$ represents the nonlinear term and $\mathbf{A}$ is a linear diagonal operator, both from $\mathbb{R}^{N/2}$ to $\mathbb{R}^{N/2}$. The k-th component of the image of each operator is given by

$$[\mathbf{r}(\widehat{\mathbf{u}}(t))]_k = -\frac{1}{2}\, i\, k\, \widehat{[u^2(t)]}_k, \quad [\mathbf{A}\widehat{\mathbf{u}}(t)]_k = -\nu\, k^{2\alpha}\, \widehat{u}_k(t), \quad k = 1, ..., N/2,$$

where $\left\{\widehat{[u^2(t)]}_k\right\}_k$ denote the Fourier coefficients of the function $u^2(t, x)$. The Fourier coefficients are computed using the `FFTW` library and this is the reason why we consider N as some power of 2. This is a standard choice for the resolution to guarantee an efficient computation of the Fourier coefficients using the Fast Fourier Transform (FFT). To avoid the aliasing phenomenon, we use the "3/2 rule" [Pey02].

The integration in time will be performed by a hybrid method combining the

Crank-Nicolson (CN) method with a three-step Runge-Kutta (RK) method. The scheme is given by

$$\left(I - \frac{h_{rk}}{2}\mathbf{A}\right)\widehat{\mathbf{u}}^{rk+1} = \widehat{\mathbf{u}}^{rk} + \frac{h_{rk}}{2}\mathbf{A}\widehat{\mathbf{u}}^{rk} + h_{rk}\beta_{rk}\mathbf{r}(\widehat{\mathbf{u}}^{rk}) + h_{rk}\zeta_{rk}\mathbf{r}(\widehat{\mathbf{u}}^{rk-1}), \qquad (3.4)$$

where $rk = 1, 2, 3$ and

$$h_1 = \tfrac{8}{15}\Delta t, \quad h_2 = \tfrac{2}{15}\Delta t, \quad h_3 = \tfrac{1}{3}\Delta t,$$

$$\beta_1 = 1, \qquad \beta_2 = \tfrac{25}{8}, \qquad \beta_3 = \tfrac{9}{4},$$

$$\zeta_1 = 0, \qquad \zeta_2 = -\tfrac{17}{8}, \qquad \zeta_3 = -\tfrac{5}{4}.$$

In this scheme, $\widehat{\mathbf{u}}^1$ and $\widehat{\mathbf{u}}^4$ represent the solutions of system (3.3) at the current and future time, respectively. We will be referring to this numerical method as CNRK3. Important features to highlight concerning the numerical method (3.4) are an explicit and an implicit treatment of the nonlinear and linear part of equation (3.3a), respectively. Deduction of the numerical method can be found in [Bew09]. The order of convergence of the CNRK3 method is two which is the order of convergence of the less accurate method between CN and RK3. As regards stability, we require the time step to be small enough, i.e. we will ask that

$$\Delta t \le C \left(\Delta x\right)^\eta, \qquad (3.5)$$

where C is a constant, $\eta \in \{1, 2\}$ and, Δt and Δx are the grid sizes in time and space, respectively. The choice of η depends on the numerical method. If it is explicit, then

16

$\eta = 2$, otherwise $\eta = 1$.

3.1.1 Grid refinement

Since one of our goals is to approximate solutions of system (2.1) in the supercritical region near the time of blow-up, it will be necessary to use a large number N of Fourier coefficients. However, it is a waste of time and computational resources to start solving the partial differential equation (PDE) with a fine resolution, because at early times, usually when smooth initial data is used, just a small number of Fourier coefficients are significant. This is why we have implemented an automatic grid refinement.

Let us recall that the spatial grip size is $\Delta x = 2\pi/N$ and the time step is $\Delta t = \mathcal{O}(1/N)$, where N is the resolution. Then, increasing the resolution N will produce a refinement in space and time. So, the main idea is to start solving the PDE with a coarse resolution and then, as the solution develops small-scale features, gradually increase the resolution using certain criteria in terms of the spectrum of the solution.

We say that the spectrum is completely developed if the exponential decay of the Fourier coefficients can be properly observed. An example of a fully developed spectrum is shown in figure 3.1a given by $*$. We notice that the tail of the spectrum retains a lot of Fourier coefficients which are at the level of the machine precision. Therefore, in addition to de-aliasing, we apply a sharp low-pass filter to the spectrum to set them zero. To do that, we fix a threshold around 10^{-17}, and almost every Fourier coefficient with an absolute value under that value will become zero. This step prevents the accumulation of round-off errors in the solution (see figure 3.1b).

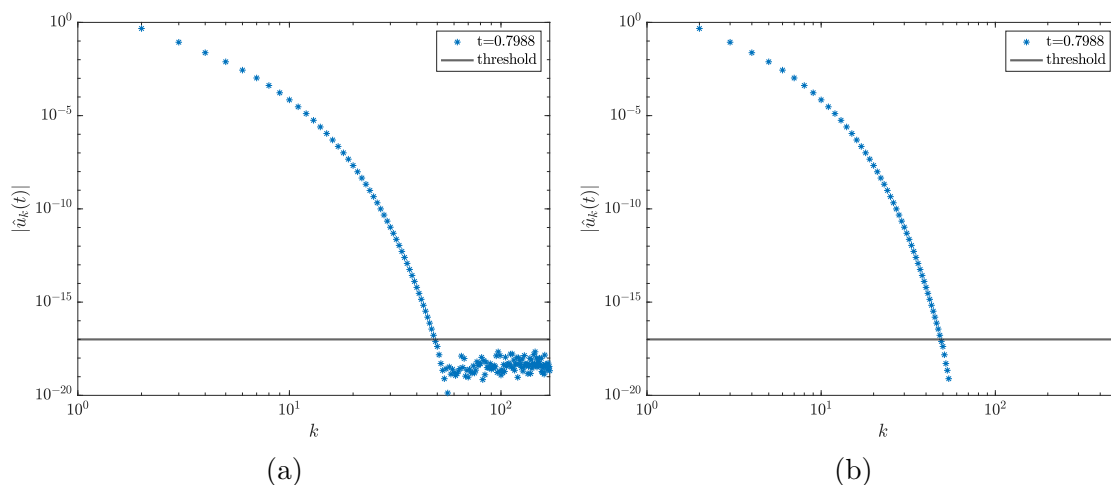(a)   (b)

Figure 3.1: Spectrum of the solution of equation (3.3) at $t = 0.3887$ with a resolution of $N = 2^9$, $\nu = 0.11$, $\alpha = 0.3$ and $g(x) = \sin(x)$ as the initial condition before (a) and after (b) applying a low-pass filter. Black line in both graphs stands for the level of the threshold at 10^{-17}.

If the low-pass filter modifies the spectrum, it indicates that the spectrum is fully developed. Otherwise, it means that the spectrum is above the threshold that we previously fixed and a refinement will be applied. By refinement we mean to increase the resolution by a factor of 2 and complete the spectrum by adding zeros at the previous time step. That is essentially the refinement condition which is checked in every time step. In figure 3.2a, a case where the refinement is necessary is presented. We considered a threshold at 10^{-17}. Note that the solution is not fully resolved with $N = 2^9$, because the whole spectrum is above this threshold. Then a refinement is applied by doubling the resolution from 2^9 to 2^{10}, in order to see the complete exponential decay in the Fourier coefficients (see figure 3.2c). After this, the filter is applied again and the procedure goes on. (See algorithm 1)
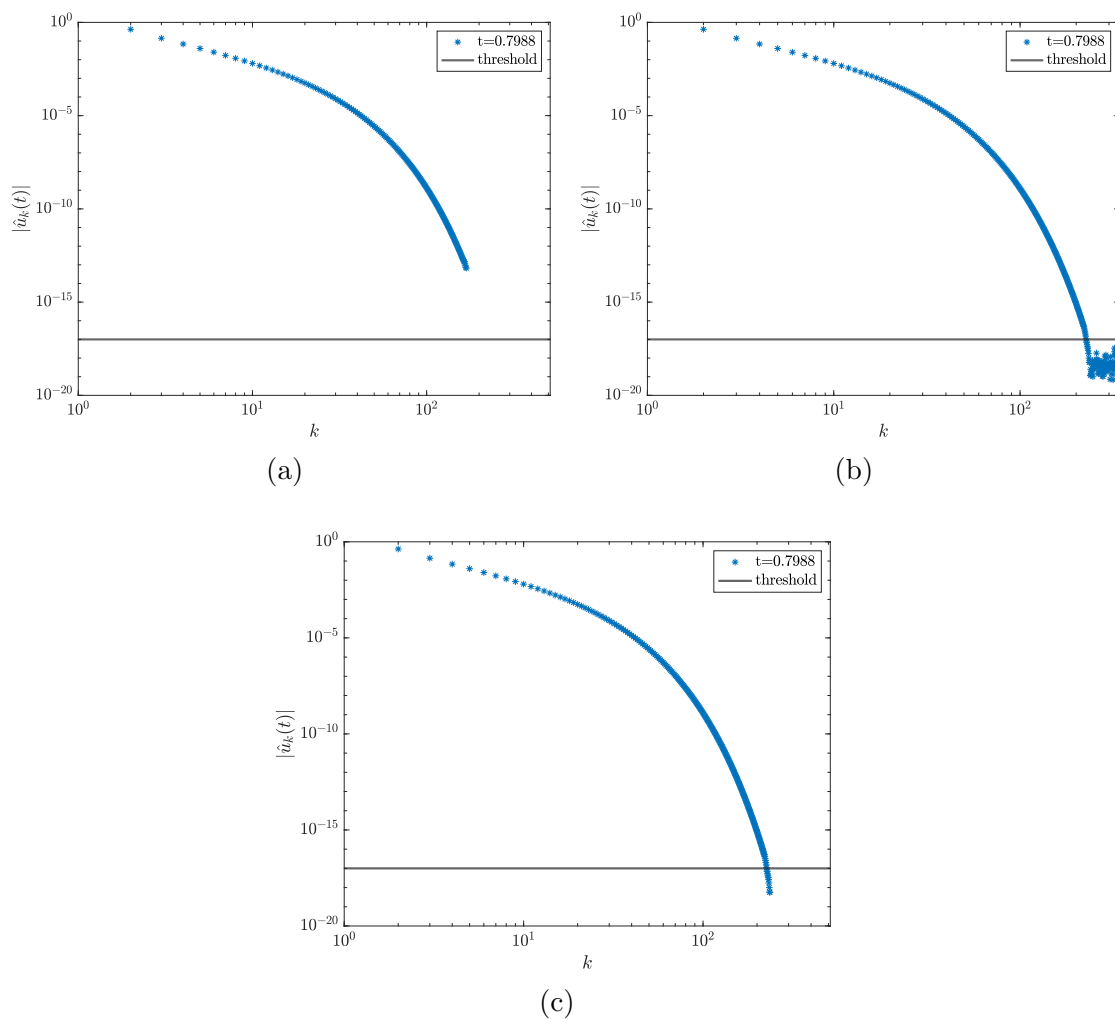
(a)

(b)

(c)

Figure 3.2: Spectrum of the solution of the system (3.3) at $t = 0.7988$ with $\nu = 0.11$, $\alpha = 0.3$ and $g(x) = \sin(x)$ as the initial condition with resolution (a) $N = 2^9$ and (b) $N = 2^{10}$. Filtered solution with resolution $N = 2^{10}$ is presented in panel (c). Black line in all three plots stands for the level of the threshold at 10^{-17}.

Algorithm 1: Grid refinement at a given time step t_i

---

1 Input: $\left[\widehat{u}_1(t_i), \widehat{u}_2(t_i), ..., \widehat{u}_{N/2}(t_i)\right]$, N, *threshold*.

2 Step 1: Follow the decreasing pattern of the Fourier coefficients up to the coefficient where the spectrum is not decreasing anymore. Let us say it is the coefficient $\widehat{u}_l(t_i)$, $l \leq N/2$.

3 Step 2: Refinement condition:

4 if $|\widehat{u}_l(t_i)| > threshold$ **then**

5   %Refinement is applied.

6   Increase N by a factor of two. Complete the spectrum at the previous time step t_{i-1} and solve for $t = t_{i-1} + \Delta t$.

7 else

8   % Apply the low-pass filter to the spectrum.

9   Keep the same N and set $\widehat{u}_k(t_i) = 0$, $k = l+1, ..., N/2$.

3.2 Stochastic Version of the Fractional Burgers Equation

As in the deterministic case, to solve system (2.9) numerically, we will use a Fourier-Galerkin pseudo-spectral approach. So we will consider a Fourier representation of the solution as in expression (3.1). Again, the conjugate symmetry property holds and only functions with mean zero are considered. Now, plugging expression (3.1)

in equation (2.13), we obtain

$$d\widehat{\mathbf{u}} = (\mathbf{r}(\widehat{\mathbf{u}}(t)) + \mathbf{A}\widehat{\mathbf{u}}(t))\, dt + \sigma\, d\mathbf{W}(t),$$
$$\widehat{\mathbf{u}}(0) = \widehat{\mathbf{g}},$$

(3.6)

where $\widehat{\mathbf{u}}(t)$, $\mathbf{r}(\widehat{\mathbf{u}}(t))$ and $\mathbf{A}\widehat{\mathbf{u}}$ are as in system (3.3) and $\mathbf{W}(t) = [W_1(t), ..., W_{N/2}(t)]^T$, where

$$W_k(t) = \frac{\sqrt{2}}{2k}\left(\beta_{2k}(t) - i\beta_{2k-1}(t)\right),$$

(3.7)

and $\beta_1,..., \beta_N$ are i.i.d standard Brownian motions.

Following the same idea of the numerical approach of the deterministic version of the fractional Burgers equation, we will use FFT to compute the Fourier coefficients. We will also use the "3/2 rule" to avoid the aliasing phenomenon. For the time discretization, we will use a stochastic Runge-Kutta method of order one-and-half studied in [Cha87]. The scheme is given by

$$\mathbf{Q}^{(n)} = \widehat{\mathbf{u}}^n + \frac{1}{2}\Delta t\,\mathbf{f}(\widehat{\mathbf{u}}^n),$$
$$\mathbf{Q}^{*(n)} = \widehat{\mathbf{u}}^n + \frac{1}{2}\Delta t\,\mathbf{f}(\widehat{\mathbf{u}}^n) + \frac{3}{2}\sigma\sqrt{\Delta t}\,\boldsymbol{\beta},$$
$$\widehat{\mathbf{u}}^{n+1} = \widehat{\mathbf{u}}^n + \sigma\Delta\mathbf{W}^n + \frac{1}{3}\Delta t\left[\mathbf{f}(\mathbf{Q}^n) + 2\mathbf{f}(\mathbf{Q}^{*(n)}))\right]$$

(3.8)

where $\widehat{\mathbf{u}}^n$ stands for the solution of system (3.6) at the n-th time step, Δt is the size of the time step, $\mathbf{f}(\widehat{\mathbf{u}}) = \mathbf{r}(\widehat{\mathbf{u}}(t)) + \mathbf{A}\widehat{\mathbf{u}}(t)$, $\boldsymbol{\beta}$ is a suitable $\mathbb{C}^{N/2}$-valued random variable, $\Delta\mathbf{W}^n = \mathbf{W}^{n+1} - \mathbf{W}^n$ and $\mathbf{W}^n$ is the noise at the n-th time step. To compute $\Delta\mathbf{W}^n$ and $\boldsymbol{\beta}$ we follow the steps:

i. Consider $\boldsymbol{\xi}$ and $\boldsymbol{\eta}$ as two independent $\mathbb{C}^{N/2}$-valued Gaussian variables with distribution $\mathcal{N}(0, I_{N/2})$,where $I_{N/2}$ is the identity matrix of size $N/2 \times N/2$.

ii. Set $\Delta \mathbf{W}^n = \sqrt{\Delta t}\,\boldsymbol{\xi}$ and $\boldsymbol{\beta} = \frac{1}{2}\boldsymbol{\xi} + \frac{\sqrt{3}}{6}\boldsymbol{\eta}$.

Regarding the stability, we are again under the rule (3.5).

3.2.1 Grid refinement

For the same reason as already presented in section 3.1.1, it will be necessary to consider a large number N of Fourier coefficients. Therefore, an automatic increasing of resolution was implemented when solving the stochastic fractional Burgers equation.

Before mentioning the algorithm we used, it is necessary to understand how the spectrum of the solution evolves in the stochastic fractional Burgers equation. Two examples were plotted in figure 3.3. Both plots correspond to the same values of the parameters α, ν, the resolution N and initial condition, except for the amplitude of the noise σ. The following patterns were observed. First, a deterministic-like behavior of the spectrum for small wavenumbers k is follow by a tail dominated by the noise. In figure 3.3b, the noise has an amplitude of $\sigma = 10^{-2}$ versus an amplitude of $\sigma = 10^{-6}$ in figure 3.3a. This is why the effect of the noise is more noticeable in figure 3.3b. In the deterministic version of the fractional Burgers equation, the tail is the result of round-off errors and therefore can be removed with low-pass filtering. In the stochastic version, however, tails cannot be removed since they represent the effect of the noise of the stochastic forcing. Second, after several simulations

we identified that the noise starts dominating in the spectrum around 2 orders of magnitude below σ. For instance, we can check that the noise starts being noticeable around 10^{-8} and 10^{-4} in figures 3.3a and 3.3b, respectively. This particular feature is exactly what we are going to use as our refinement condition, as described in Algorithm 2.
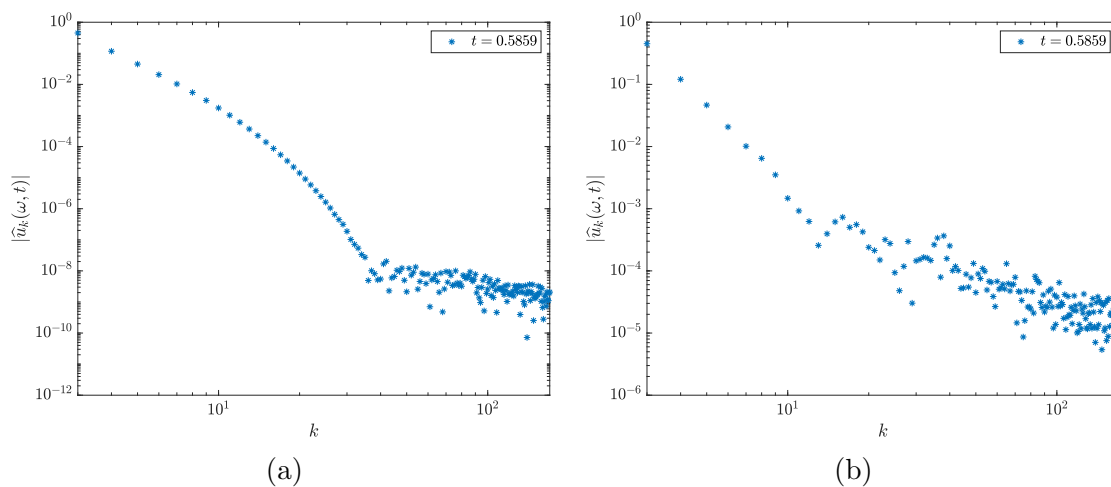

(a)   (b)

Figure 3.3: Spectrum of a single realization of the solution of system (3.6) at $t = 0.5859$ with (a) $\sigma = 10^{-6}$ and (b) $\sigma = 10^{-2}$. The other parameters are the resolution of $N = 2^9$, $\nu = 0.11$, $\alpha = 0.6$ and $g(x) = \sin(x)$ as the initial condition.

Algorithm 2: Grid Refinement For Stochastic Version at Time t_i

---

1 Input: $\left[\widehat{u}_1(t_i), \widehat{u}_2(t_i), ..., \widehat{u}_{N/2}(t_i)\right]$, N, σ.

2 Step 1: Create a threshold depending on σ.

3 $threshold = \sigma\, 10^{-2}$.

4 Step 2: Follow the deterministic-like behavior of the spectrum until it

 reaches the tail dominated by the noise at $|\widehat{u}_l(t_i)|$ for some $l \leq N/2$.

5 Step 3: Apply the refinement condition.

6 if $|\widehat{u}_l(t_i)| > threshold$ **then**

7 | Increase N by a factor of two. Complete the spectrum at the previous

  | time step t_{i-1} and solve for $t = t_{i-1} + \Delta t$.

8 else

9 | Keep the same N

A key difference between Algorithms 1 and 2 is how we complete the spectrum when a refinement is needed. For the deterministic case, we add zeros since the tail of the spectrum contains Fourier coefficients that are no significant. On the other hand, in the stochastic version, the tail of the spectrum is not at the level of the machine precision, which is due to the slow decay of the noise in the Fourier space. Thus, consistently with the pattern observed in Figure 3.3, the spectrum is completed with random Fourier coefficients decaying with k at a suitable rate.

After implementing this adaptive refinement, we found out that making a grid refinement to the spectrum, when the tail of Fourier coefficients is not at the level of the machine precision, will carry some problems in the computation of the enstrophy. As we just mentioned, every time we applied a grid refinement in the stochastic case,

the spectrum would be completed with noise. Therefore, as the amplitude of the noise σ increases, the noise we add is significant in the computation of the enstrophy, and that will make that the enstrophy suddenly jumps every time a refinement is made. Unlike the stochastic case, grid refinement makes sense in the deterministic case because even for coarse resolutions, the tail of the spectrum is at the level of the machine precision, so adding zeros to the spectrum is not going to alter the enstrophy.
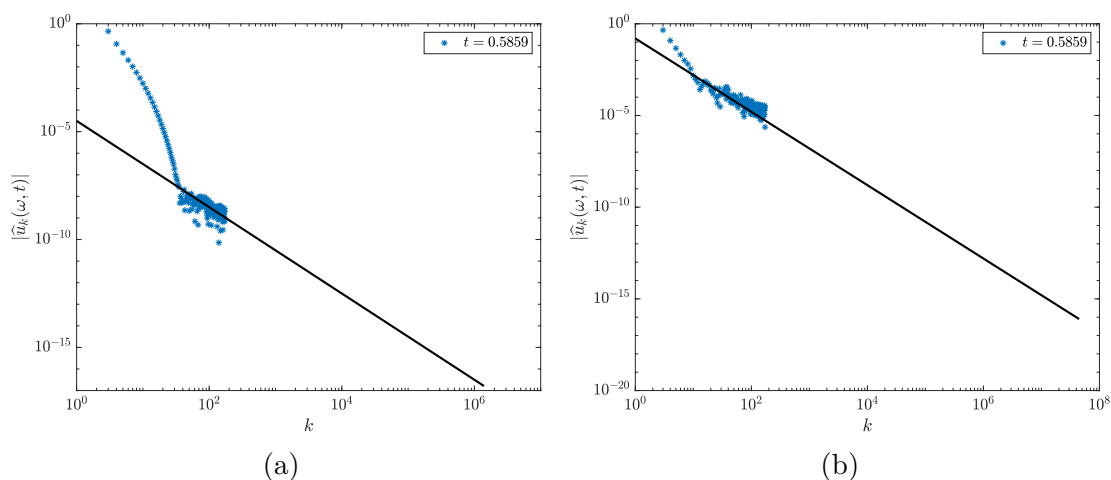

Figure 3.4: Blue symbols in panels (a) and (b) represent the same information as in figures 3.3a and 3.3b, respectively. Black lines show the projected level of the tail if the resolution increases up to $N = 2^{22}$ in (a) and $N = 2^{30}$ in (b).

If we want to apply the grid refinement as in the deterministic case, we need to start solving system (2.9) with a resolution large enough to make the Fourier modes reach the machine precision level. If we are solving the stochastic system (2.9) with an amplitude of the noise of $\sigma = 10^{-6}$ and $\sigma = 10^{-2}$, Figures 3.4a and 3.4b give an idea about the resolution needed to reach that level, respectively. In the case

of figure 3.4a, the black line is the projected tail with a resolution of $N = 2^{22}$ and for the case in figure 3.4b, the black line is the projected tail with a resolution of $N = 2^{30}$. It is clear that the time to compute the solution of system (2.9) starting at these resolutions will be very long. Therefore, we decided to work with a fixed "medium size" resolution of $N = 2^{17}$.

3.3   Evaluation of Diagnostic Quantities

To compute the diagnostic quantities, we proceed as follows. First, we used the Parseval's identity to find the enstrophy in the Fourier space

$$\mathcal{E}(t) = \pi \int_0^{2\pi} |\partial_x u(t,x)|^2 \, dx = 2\,\pi^2 \sum_{k=-\infty}^{\infty} k^2 |\widehat{u}_k(t)|.^2 \tag{3.9}$$

Due to the conjugate symmetry property and the truncation of the solution with N Fourier modes, then we can approximate the enstrophy as

$$\mathcal{E}(t) \sim 4\,\pi^2 \sum_{k=1}^{N/2} k^2 |\widehat{u}_k(t)|.^2 \tag{3.10}$$

For the width of the analyticity strip, we use a method developed in [AP11]. In agreement with Theorem 2.4, it assumes that the spectrum can be expressed as

$$|\widehat{u}_k(t)| \sim C(t)\,|k|^{\tilde{\alpha}(t)} e^{-\delta(t)\,k}, \tag{3.11}$$

where $\delta(t)$ is the width of the analyticity strip of $u(t, x)$, $\tilde{\alpha}(t)$ is the order of the nearest complex singularity and $C(t)$ is an adjustable parameter. An estimate of $\delta(t)$ can be then obtained by minimizing the least-squares error between ansatz (3.11) and the spectrum of $u(t, x)$. The usual procedure is to consider the function

$$f(k) = \ln(C) + \tilde{\alpha} \ln(|k|) - \delta\, k - \ln(|\widehat{u}_k|), \tag{3.12}$$

and solve the optimization problem

$$\min_{(C,\tilde{\alpha},\delta)\in\mathbb{R}^3} \sum_{k=1}^{N/2} |f(k)|^2. \tag{3.13}$$

The advantage of using the function (3.12) is the linear dependence on the parameters $\ln(C)$, $\tilde{\alpha}$, and δ, making (3.13) a convex optimization problem. Problem (3.12)-(3.13) can be solved at discrete time steps t_i, $i = 1, ..., M$, $M \in \mathbb{N}$, allowing us to determine how the width of the anlyticity strip $\delta = \delta(t)$ depends on time. The width of the analyticity strip will be computed only for the solutions of the deterministic problem, as in the stochastic case the solutions are in general not analytic.

3.4   Estimates of the blow-up time

One of the main aims of this thesis is to understand how the blow-up time T^* depends on the fractional dissipation exponent α for a certain initial condition. In this section we focus only on the supercritical case which is where blow-up is expected to occur. We need to estimate T^* and to do that, we will follow the ideas presented in

[BB12, BK08]. We are going to suppose that the enstrophy $\mathcal{E}(t)$ and the width of the analyticity strip $\delta(t)$ locally behave as power-law functions of the form $c\,(T^* - t)^\gamma$, for $0 < t < T^*$, where T^* is the estimate of the blow-up time and c and γ are adjustable parameters, such that $\gamma > 0$ and $\gamma < 0$ when representing, respectively, $\delta(t)$ and $\mathcal{E}(t)$. Let us consider a family of sliding time windows $I_j \subset [0, T^*)$, centered at t_j, such that $t_j < t_{j+1}$ (i.e. the window I_j is sliding towards longer times as the index j increases). We define $T^*_{\mathcal{E}}(t_j)$ as the value of the parameter T^* obtained when we fit $c\,(T^* - t)^\gamma$ to the function $\mathcal{E}(t)$, $t \in I_j$. The estimate of the blow-up time $T^*_{\mathcal{E}}(t_j)$, $j = 1, ..., M$ is a function of the position of the window I_j as it moves towards the blow-up time. The estimate $T^*_{\delta}(t_j)$ is computed analogously by fitting $c\,(T^* - t)^\gamma$ to the function $\delta(t)$, $t \in I_j$. The idea of creating a family of sliding time windows is to check that the sequence of $T^*(t_j)$, $j = 1, ..., M$ converges as t_j tends to the final discrete time reached in the solution of the PDE problem

The procedure to compute $T^*_{\mathcal{E}}(t_j)$ based on enstrophy $\mathcal{E}(t)$ is as follows

---

Algorithm 3: Estimation of $T_{\mathcal{E}}^*$

---

1 Input: $\mathcal{E}(t_i)$, $i = 1, ..., q$, where q is the number of discrete time steps.

2 Output: $T_{\mathcal{E}}^*(t_j)$, $j = 1, ..., M$, where M is the number of sliding time windows.

3 Step 1: Set $j = 1$ and assume $\mathcal{E}(t_i) \approx c \, (T^* - t_i)^\gamma$, $t_i \in I_j$.

4 Step 2: consider the function obtained by applying the natural logarithm to both sides to the above expression

$$f(t_i) = \ln(c) + \gamma \ln\left(T^* - t_i\right) - \ln\left(\mathcal{E}(t_i)\right), \quad t_i \in I_j.$$

5 Step 3: Obtain estimates $T^*(t_j)$, $c(t_j)$ and $\gamma(t_j)$ by solving the least-square minimization problem

$$\min_{(c,\gamma,\mathbb{T}^*) \in \mathbb{R}^3} \sum_{t_i \in I_j} |f(t_i)|^2.$$

6 Step 4: Make $j = j + 1$ (slide the window).

3.5   Software Implementation

For the deterministic case, all computations and post-processing of the data was done using MATLAB. The optimization problems in expression (3.13) and in Algorithm 3 were solved using the function `fminsearch`. On the other hand, in the stochastic case, computations were performed in Julia which accelerated performance as compared to MATLAB. The optimization problems were solved using the function `optimize` from the package `Optim`. However, postprocessing and visualizations of the data were

still performed in MATLAB.

Chapter 4

Results

In this chapter we are going to illustrate the solutions of systems (2.1) and (2.9) based on the numerical methods we discussed in the previous chapter. First, we will focus on the deterministic case and will also present the diagnostic quantities for different values of the dissipation fractional exponent α, as well as the estimates of the blow-up time T^* computed with Algorithm 3. Then, we will check that the obtained estimates are consistent with some limiting cases. In the second part of this chapter we will focus on the stochastic case.

4.1 Deterministic Case

Motivated by the discussion in Section 2.1, we will consider the deterministic problem (2.1) in the subcritical regime with $\alpha = 0.8$ and in the supercritical regime with $\alpha = 0.3$ and $\alpha = 0.1$. Unless it is indicated otherwise, the initial condition and the viscosity are the same in all cases and given by $g(x) = \sin(x)$ and $\nu = 0.11$. The
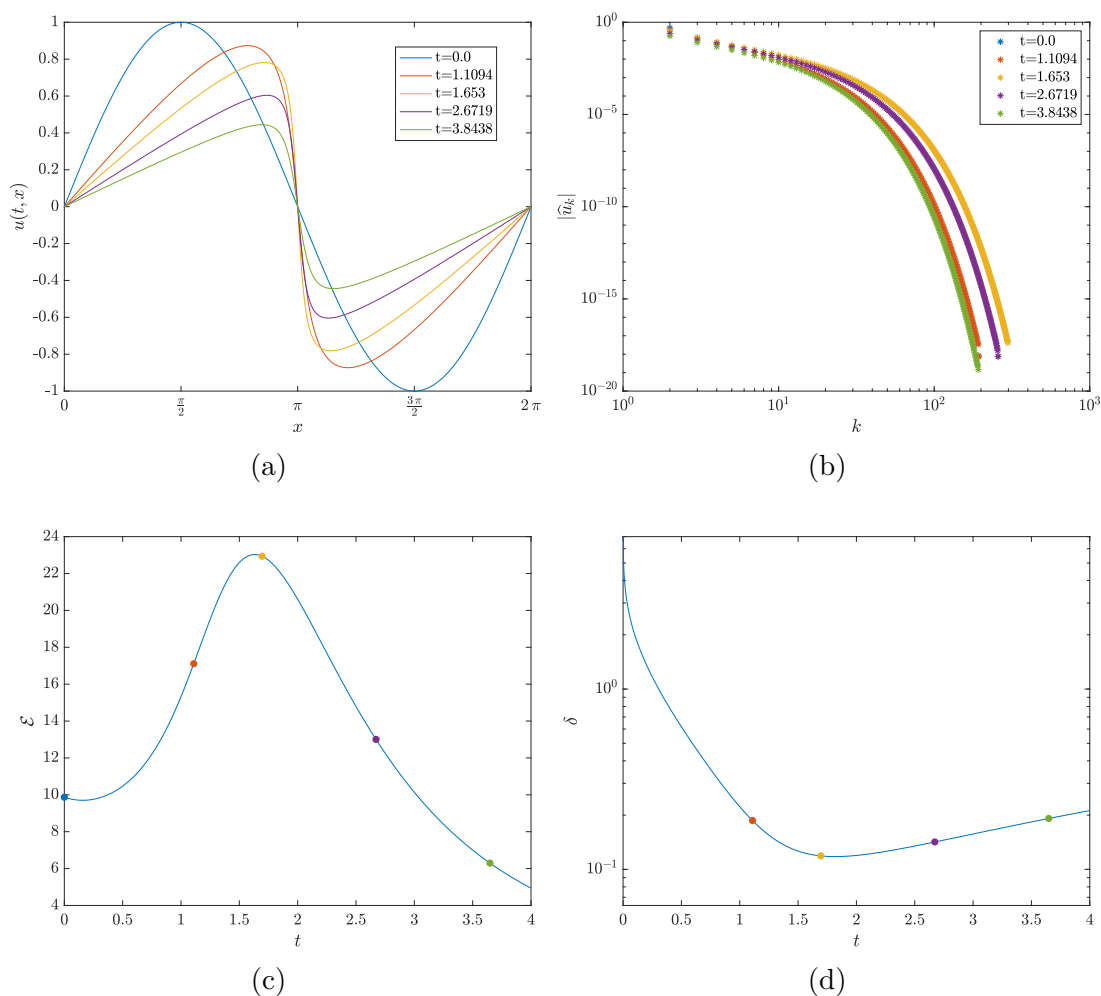
Figure 4.1: Solution of system (2.1) with $\alpha = 0.8$ in (a) the physical space $u(t,x)$ and (b) the Fourier space $|\widehat{u}_k(t)|$ with the corresponding evolution of (c) the enstrophy $\mathcal{E}(t)$ and (d) the width of the analyticity strip $\delta(t)$. The symbols in panel (c) and (d) correspond to the time instances at which the solution is shown in panels (a) and (b).

problem is solved using CNRK3 approach described in Section 3.1 with adaptive resolution varying from $N = 2^9$ to $N = 2^{18}$ in the supercritical case and from
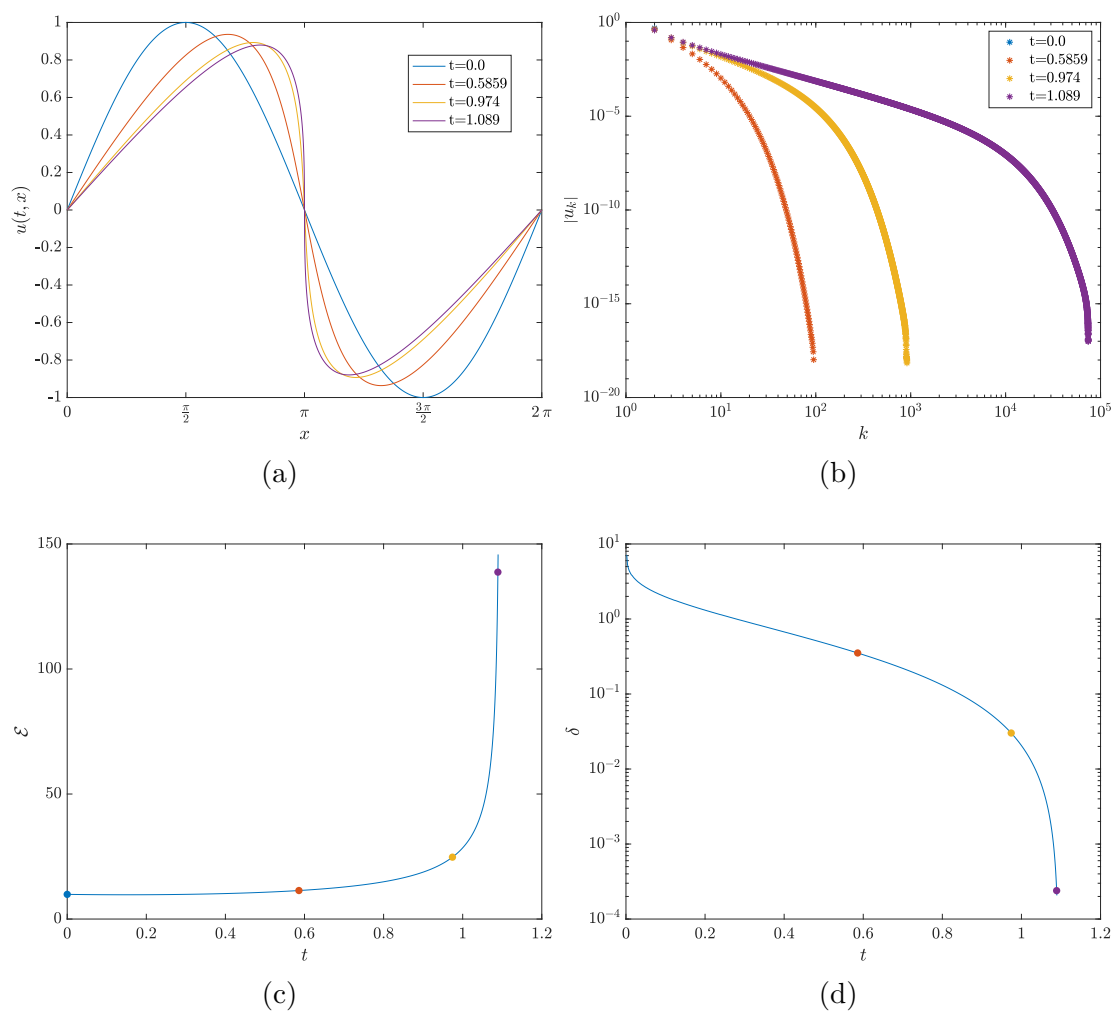
Figure 4.2: Solution of system (2.1) with $\alpha = 0.3$ in (a) the physical space $u(t, x)$ and (b) the Fourier space $|\widehat{u}_k(t)|$ with the corresponding evolution of (c) the enstrophy $\mathcal{E}(t)$ and (d) the width of the analyticity strip $\delta(t)$. The symbols in panel (c) and (d) correspond to the time instances at which the solution is shown in panels (a) and (b).
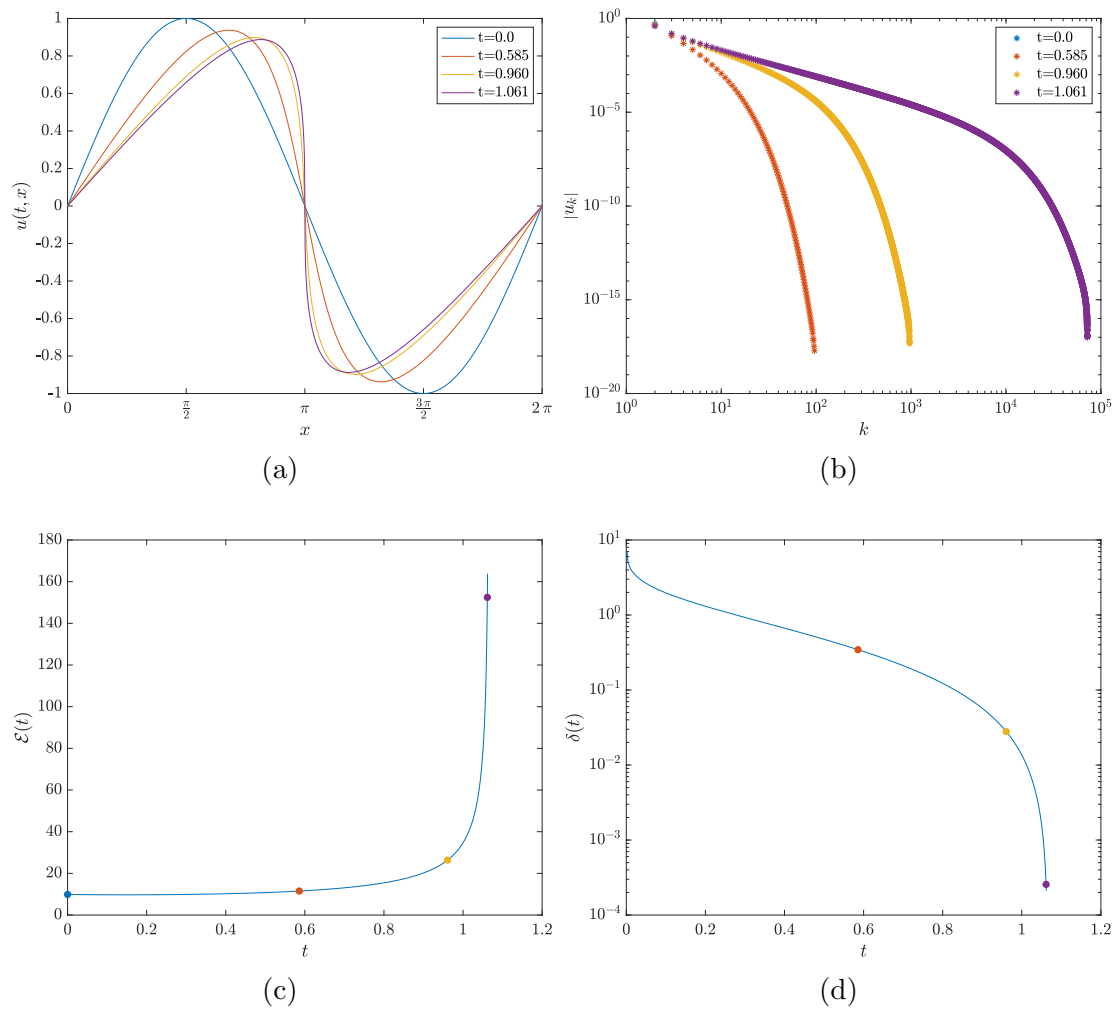
Figure 4.3: Solution of system (2.1) with $\alpha = 0.1$ in (a) the physical space $u(t, x)$ and (b) the Fourier space $|\widehat{u}_k(t)|$ with the corresponding evolution of (c) the enstrophy $\mathcal{E}(t)$ and (d) the width of the analyticity strip $\delta(t)$. The symbols in panel (c) and (d) correspond to the time instances at which the solution is shown in panels (a) and (b).

$N = 2^9$ to $N = 2^{22}$ for the subcritical case. However, for this last case, It was not always necessary to achieve this upper bound for the resolution.

The solution in the physical and Fourier space, the enstrophy and the width of the analyticity strip are shown in figures 4.1, 4.2 and 4.3. The first one is in the subcritical regime while the last two are in the supercritical regime. Figures 4.1a, 4.2a and 4.3a exhibit classical interactions between the dissipation and the nonlinear terms in system (2.1) in the physical space. For figure 4.1a, in early times the nonlinear factor dominates the dissipative term and therefore the front of the solution starts steeping. However, the dissipative term eventually overcomes the nonlinear factor and the front starts to flatten. On the other hand, figures 4.2a and 4.3a show the superiority of the nonlinear term of equation (2.1a), which leads to the formation of shocks and therefore singularities at a finite time. Figures 4.1b, 4.2b and 4.3b illustrate the solutions in the Fourier space. In figure 4.1b, we can note that just a small number of Fourier coefficients are needed to completely solved problem (2.1) in the subcritical regime, while figures 4.2b and 4.3b show that as the time increases, more and more Fourier coefficients are required. The enstrophy in panels 4.1c, 4.2c and 4.3c shows what is expected. It is bounded when the solution is smooth and unbounded when a singularity a finite time is formed. Lastly, the width of the analyticity strip is presented in figures 4.1d, 4.2d and 4.3d, where we can observed the formation of singularities in the supercritical case and its boundedness above zero for smooth solutions.

The relevance of figure 4.3 is that it provides numerical evidence that the solution of system (2.1) blows up in $H_p^1(0, 2\pi)$ for a value of α outside of the condition stated

in Theorem 2.3 and a particular initial condition given by $g(x) = \sin(x)$.

To conclude this section, plots showing the evolution of the enstrophy and the width of the analyticity strip as the fractional dissipation exponent α moves along $[0, 1]$ are presented in figure 4.4. The critical case was excluded because it would required a very large resolution in order of capture the whole dynamics of the enstrophy, which imply excessive long time of computing.
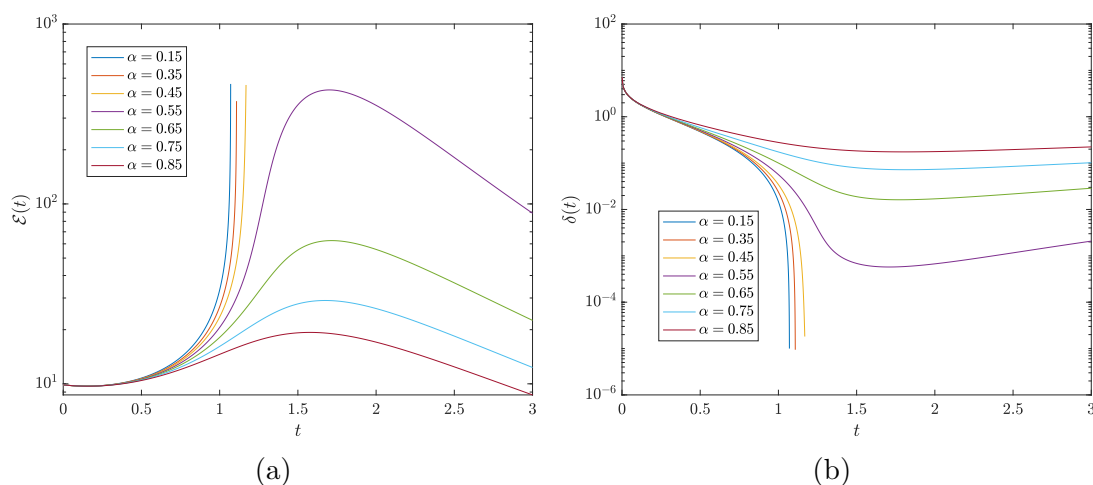

Figure 4.4: Evolution of (a) the enstrophy and (b) the width of the analyticity strip of the solution of the fractional Burgers equation for different values of the dissipation exponent.

4.1.1   Estimates of the blow-up time

Since we are going to discuss blow-up time, we will limit the parameter α only in the supercritical case $\alpha \in [0, 1/2)$ in this section. The first main result is presented in figure 4.5a. It shows estimates of the blow-up time T^* as a function of t for different values of the fractional dissipation exponent α. These estimates were obtained using

Algorithm 3 applied to both the enstrophy $(T_{\mathcal{E}}^*(t))$ and the width of the analyticity strip $(T_\delta^*(t))$.

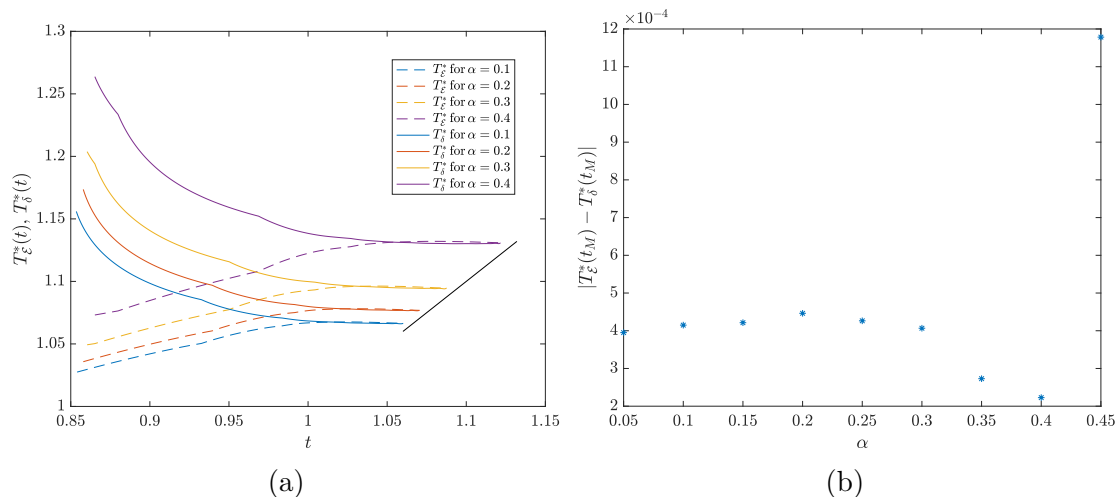(a)   (b)

Figure 4.5: (a) Estimates of the blow-up time based on the enstrophy (dashed lines $T_{\mathcal{E}}^*$) and the the width of the analyticity strip (solid lines T_δ^*) as functions of time for different values of α. Curves with the same color indicate the estimates for the same value of α. The black line correspond to $T^* = t$ and it gives us a reference of how far the estimate of T^* can be continued. If follows from the fact that we are approximating T^* over all the time where the numerical solution is defined, and the end of that domain is T^*. (b) Difference between $T_{\mathcal{E}}^*(t_M)$ and $T_\delta^*(t_M)$ of curves with the same color.

We must highlight from figure 4.5a that the two estimates of the blow-up time, based on the enstrophy and the width of the analyticity strip, converge to very similar values as the time increases. The difference between these values obtained as the last time window I_M are shown in figure 4.5b as function of α. Since these difference

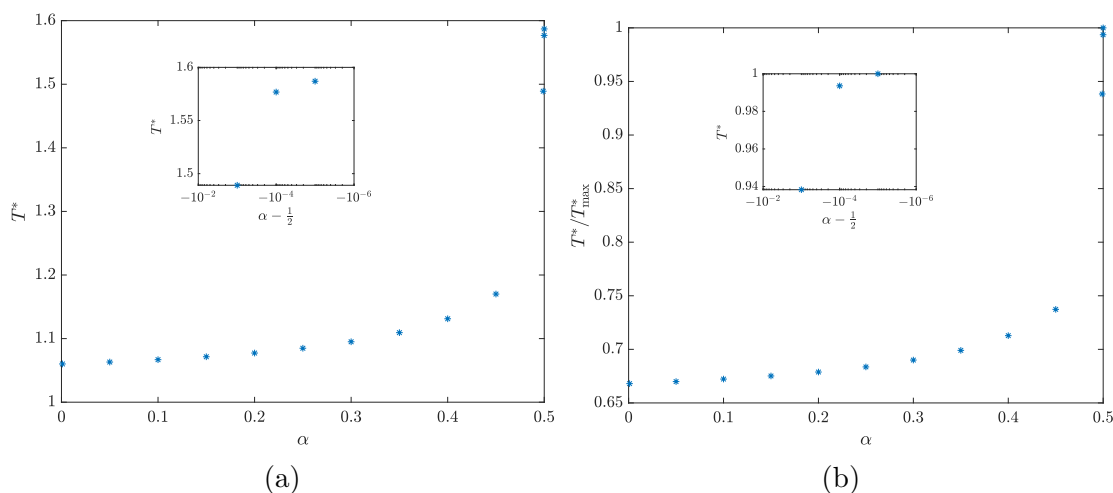(a)   (b)

Figure 4.6: (a) Estimates of the blow-up time T^* as a function of α of system (2.1) with $\nu = 0.11$, $g(x) = \sin(x)$, and the resolution ranging from 2^9 until 2^{18}. (b) Relative amplitude of the blow-up time estimates as a function of α. $T^*_{max} :=$ $\max_\alpha T^*$.

are for all α very small, on the order of $\mathcal{O}(10^{-3})$- $\mathcal{O}(10^{-4})$, we conclude that the two approaches to estimate the blow-up time are consistent. Moving forward, we will estimate the blow-up time based on enstrophy as this approach generalizes to the stochastic case. We will used the simplified notation $T^* = T^*_{\mathcal{E}}(t_M)$.

The second main result of this section is shown in figure 4.6a. It presents the blow-up time estimate T^* as a function of α. We can notice a monotonous dependence of T^* on α. The smallest and the highest considered values of α in the supercritical case were 0.001 and 0.49999, respectively. Figure 4.6b let us see that there is a relative variation of more than the 30% of the values of T^* for that range of α.

A natural question in this stage is how the results presented in figure 4.6a depend on the resolution N. To answer this question, in figure 4.7 we plot the difference be-
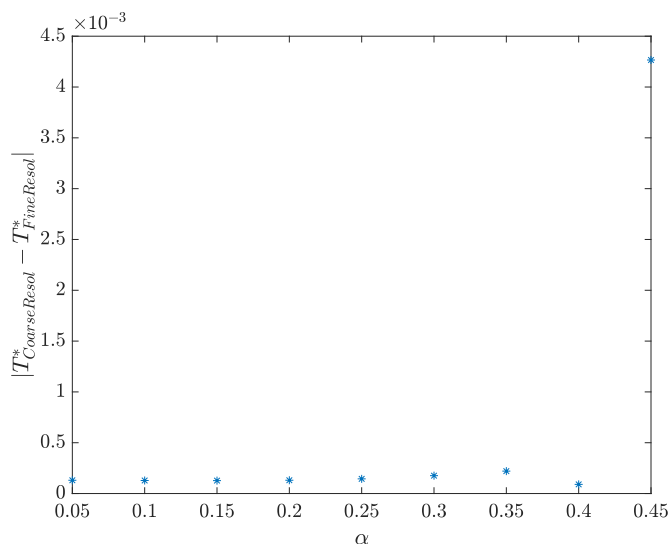
Figure 4.7: Difference between estimates of the blow-up time of system (2.1) using $\nu = 0.11$, $g(x) = \sin(x)$ with two different ranges of resolution. We denote $T^*_{FineResol}$ and $T^*_{CoarseResol}$ to the blow-up time estimates of the system (2.1) computed with resolutions starting from 2^9 until 2^{20} and 2^{18}, respectively.

tween the blow-up time T^* obtained from numerical solution with a coarse resolution ranging from $N = 2^9$ to $N = 2^{18}$ and a fine resolution from 2^9 up to 2^{20}. As we can see, that difference is $\mathcal{O}(10^{-3})$ even though the resolution was refined by a factor of 4. However, the time of computing the solution with the coarse resolution is noticeably shorter than using the fine resolution. In these two cases, the time to compute the solution of system (2.1) are given in table 4.1. Note that the time to compute the solution using the coarse resolution is almost seven times shorter than using the fine resolution. Therefore, from now on, all the simulations in the supercritical region will be done for a range of resolution from 2^9 until 2^{18}.

α	CPU time using a coarse resolution [sec]	CPU time using a fine resolution [sec]
0.1	839.24	5812.75
0.2	869.28	6029.43
0.3	935.79	7840.19
0.4	1244.1	12063.13

Table 4.1: Time of computing the solution of system (2.1) in seconds for different values of α with a coarse and a fine resolution. The machine we used has 32GB of RAM, 8 CPU(s) and a processor Intel(R) core(TM) i7-6700 CPU at 3.40 GHz.

4.1.2   Limiting cases

To check consistency of the estimates of the blow-up time, let us recall Subsection 2.1.1, where we studied limiting cases of system (2.1) corresponding to $\nu = 0$ and $\alpha = 0$. First, for $\alpha = 0$, we obtain system (2.7) for which blow-up time is given by expression (2.8).

From table 4.2, we see how the absolute error between the blow-up time estimates of the fractional Burgers equation and the exact blow-up time of the system (2.7) is very small as the fractional dissipation exponent α tends to zero. Thus, we conclude that our estimates are consistent with this limiting case.

α	$|T^*_{exact} - T^*|$
10^{-1}	0.007
5×10^{-2}	0.0033
10^{-2}	0.0008
10^{-3}	0.0002

Table 4.2: Absolute error between estimates of the blow-up time of system (2.1) using $\nu = 0.11$, $g(x) = \sin(x)$ and the blow-up time of the system (2.7) with the same initial condition ($T^*_{exact} = 1.05982$). The considered values of α are 10^{-3}, 10^{-2}, 5×10^{-2} and 10^{-1}.

Second, considering $\nu = 0$, we obtained the inviscid Burgers system (2.5) regardless the value of the dissipation fractional exponent α. For the initial condition $g(x) = \sin(x)$, the blow-up time for the inviscid Burgers system (2.5) is $T^*_{Inviscid} = 1$. Since it is independent of the parameter α, our estimate should approximate the constant function $T^*(\alpha) = 1$ as ν tends to zero. Figure 4.8, shows the absolute error between the estimates of the blow-up time in the systems 2.1 and the exact value of the blow-up time of the inviscid Burgers equation (2.5) for different values of α in the supercritical regime as ν tends to zero. Note that as ν decreases, the error rapidly decreases for all values of α, which is the expected behavior. Therefore, our estimates show consistency with the limiting cases $\alpha = 0$ and $\nu = 0$.

Regarding the limiting case when α tends to $1/2$ from the left, it is not clear what we can conclude about this case. However, from the figure 4.4, we conjecture that the blow-up is bounded as the fractional dissipation exponent moves from the
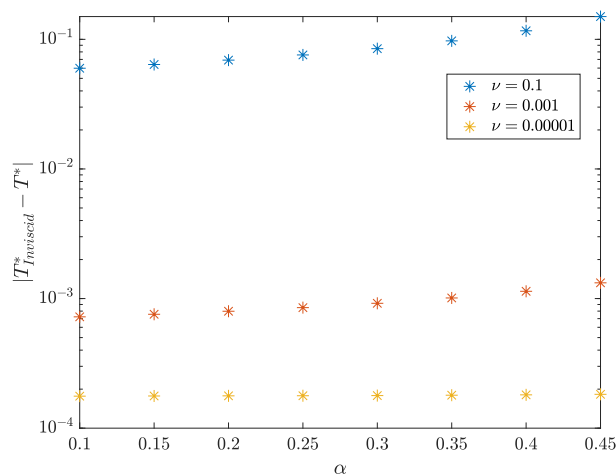
supercritical regime to $\alpha = 1/2$.

Figure 4.8: Absolute error between the estimates of T^* of system (2.1) and the blow-up time of the inviscid Burgers equation (2.5). Both using the initial condition $g(x) = \sin(x)$, different values of α in the supercritical regime and ν tending to zero. For the inviscid Burgers equation, the blow-up time occurs at $T^*_{Inviscid} = 1$ regardless the value of α.

4.2   Stochastic Case

For this section, we consider the stochastic problem (2.9) in the supercritical regime with $\alpha = 0.4$. The initial condition and the viscosity are the same as before, $g(x) = \sin(x)$ and $\nu = 0.11$. A fixed resolution of $N = 2^{17}$ is used. We are interested in the effect of the amplitude of the noise σ on the estimates of the blow-up time. In particular, in deviations of the blow-up time from the deterministic case. Since the blow-up time is a stochastic variable characterized by a certain probability distribu-

tion, it will be described in suitable terms. As we mention in Section 2.3, due to the lack of analyticity of the solution because of the noise, we are only going to use the enstrophy to estimate the blow-up time.

A single realization of the solution of system (2.9) with an amplitude of the noise $\sigma = 10^{-2}$ in the physical space is presented in figure 4.9a. The behavior of the solution is overall similar to the supercritical regime of the deterministic case of the fractional Burgers equation, i.e. a steeping front is formed, leading to a singularity at a finite time. If we take a look at the solution at small scales, the influence of the noise can be observed. Figure 4.9b shows the same solution in the Fourier space. Here, we can clearly observe the effect of the noise on the solution. We see a deterministic-like behavior followed by a tail dominated by noise. The blue $*$ symbols represents the Fourier coefficients of the initial condition, which is free of random noise. So what we observe is just roundoff errors produced by FFT applied to the initial condition. The evolution of the enstrophy is illustrated in 4.9c.

To sample the distribution of the blow-up times, we proceed with a Monte Carlo method. We apply the stochastic RK method discussed in Section 3.8 to generate several samples of the stochastic solution each obtained with a different noise sample. Then, we compute an estimate for the blow-up time for each sample as in section 3.4.

Recall that the *mean* and the *variance* of a discrete random variable X are given by

$$\mu = E[X] = \frac{1}{K} \sum_{i=1}^{K} X_i \text{ and } \widetilde{\sigma} = E\left((X - \mu)^2\right), \tag{4.1}$$

respectively, where K is the total number of realizations X_i of the random variable
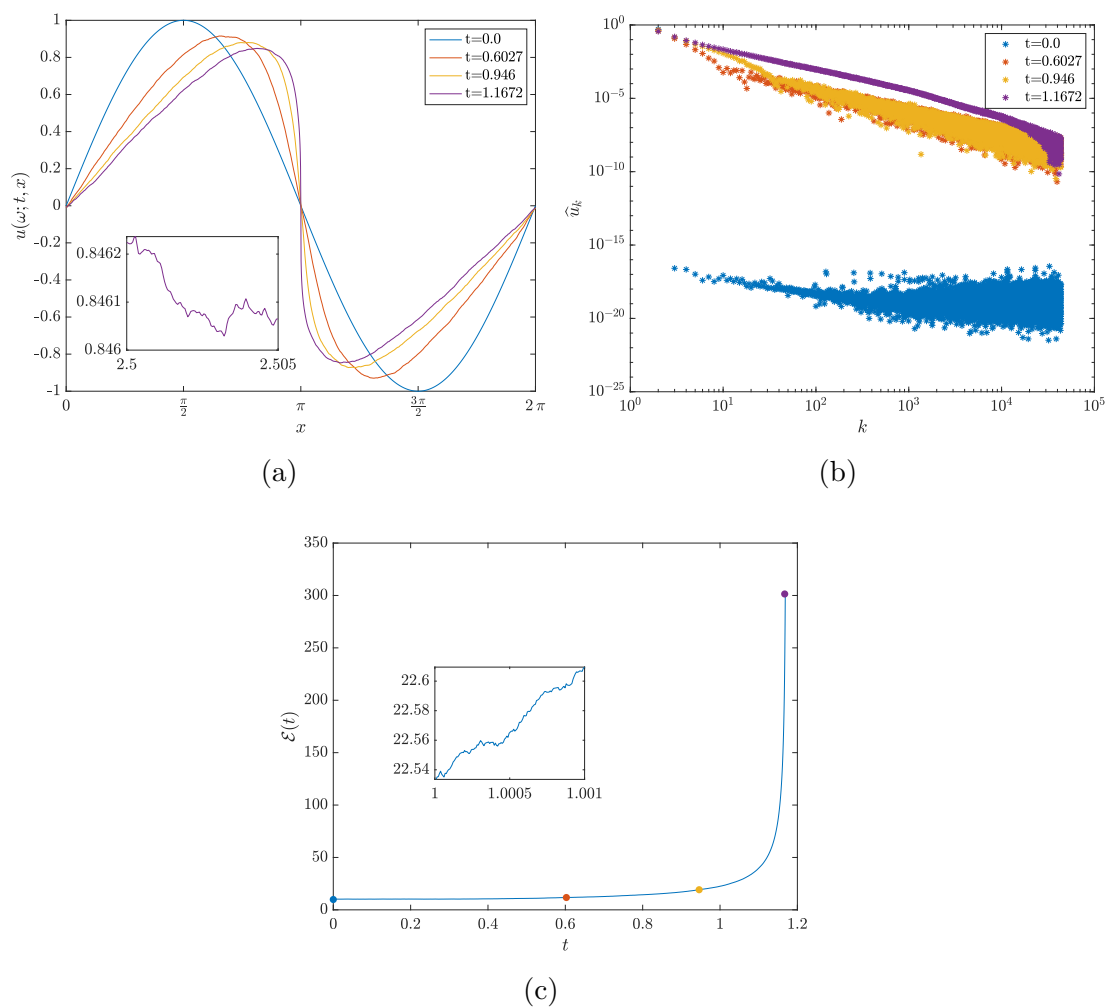
(a)

(b)

(c)

Figure 4.9: A single realization of the solution of system (2.9) with $\alpha = 0.4$, $\nu = 0.11$, $\sigma = 10^{-2}$ and fixed resolution $N = 2^{17}$. In (a) the physical space and (b) the Fourier space $|\widehat{u}_k(t)|$ with the corresponding evolution of (c) the enstrophy $\mathcal{E}(t)$. The symbols in panel (c) correspond to the time instances at when the solution is shown in panels (a) and (b).

X. In figure 4.10a the accumulated mean of the random variable T^* is shown for different values of the noise amplitude σ. We observed that as the amplitude of the
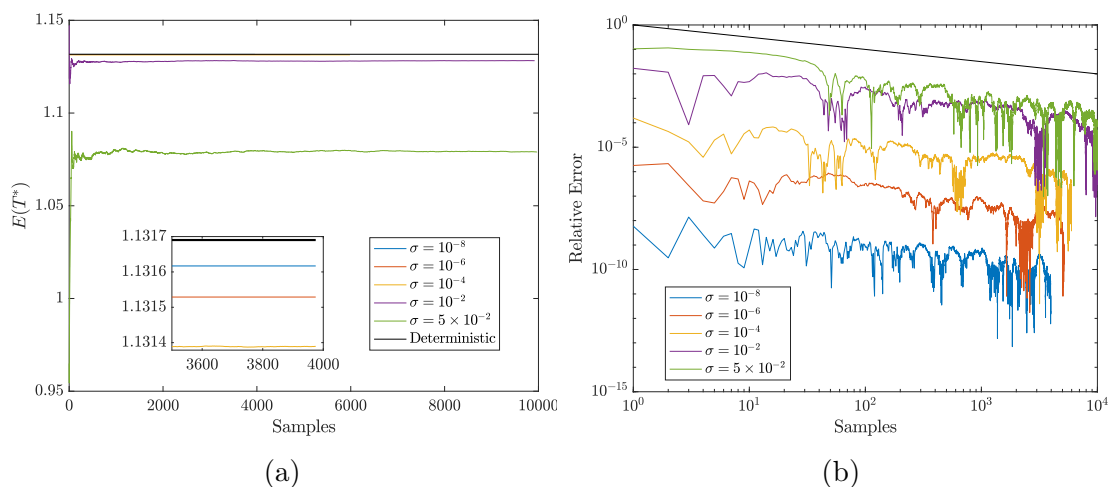
Figure 4.10: (a) Accumulate mean of the blow-up time estimate for different amplitudes of the noise. The black line in panel (a) corresponds to the blow-up time estimate in the deterministic case with $\alpha = 0.4$. (b) Relative errors of the accumulated mean of the blow-up time estimate for different amplitudes of the noise. The black curve in panel (b) describes the function $y = 1/\sqrt{x}$. We used 10000 samples for $\sigma = 5 \times 10^{-2}$ and $\sigma = 10^{-2}$, 6000 for $\sigma = 10^{-4}$, 5000 for $\sigma = 10^{-6}$ and 4000 for $\sigma = 10^{-8}$.

noise σ increases, the mean of the blow-up time decreases. In addition, the blow-up in the solution of the stochastic case tends to happen earlier in comparison to the blow-up time in the deterministic case. In figure 4.10b, the relative error respect to the accumulated mean blow-up time at the realization K is presented. As it was expected, the error slowly decreases due to the slow rate of convergence of Monte Carlo methods $\left(\mathcal{O}\left(1/\sqrt{K}\right)\right)$. This implies that as σ increases, it is necessary to consider large amount of samples in order to achieve small errors.

The distribution of the blow-up times obtained for different values of the noise

45

amplitude σ are shown in the form of histograms in figure 4.11. In order to understand the properties of these distribution, we compare them to the normal (Gaussian) distribution given by the expression

$$f(x, \mu, \sigma) = \frac{1}{\sqrt{2\pi\,\widetilde{\sigma}^2}} \exp\left[-\frac{(x-\mu)^2}{2\,\widetilde{\sigma}^2}\right], \tag{4.2}$$

where μ is the mean and $\widetilde{\sigma}$ is the standard deviation of certain set of samples computed as in expression (4.1). From figure 4.11, we can infer that as σ decreases, the distribution of the blow-up times is well approximated by the normal distribution (4.2). In order to further characterize the properties of this distribution more moments are required. The third and fourth moments, also known as *skewness* and *kursosis*, respectively, are defined as

$$skewness = E\left[\left(\frac{X-\mu}{\widetilde{\sigma}}\right)^3\right] \quad \text{and} \quad kurtosis = E\left[\left(\frac{X-\mu}{\widetilde{\sigma}}\right)^4\right], \tag{4.3}$$

where μ and $\widetilde{\sigma}$ are as in expression (4.2). This quantities are displayed in figure 4.12 together with the mean and the variance. All of them as a function of the noise amplitude σ.

From figures 4.11, 4.12c and 4.12d, we can infer that as the amplitude of the noise increases, the data start becoming more asymmetric and non-gaussian, with more probable atypical values far away in the right-hand side of the mean value of the distribution. Figure 4.11d shows that for some realizations, the noise remarkably delayed the time when the singularity shows up in comparison with the deterministic case. We believe that more data need to be added to extract useful information from
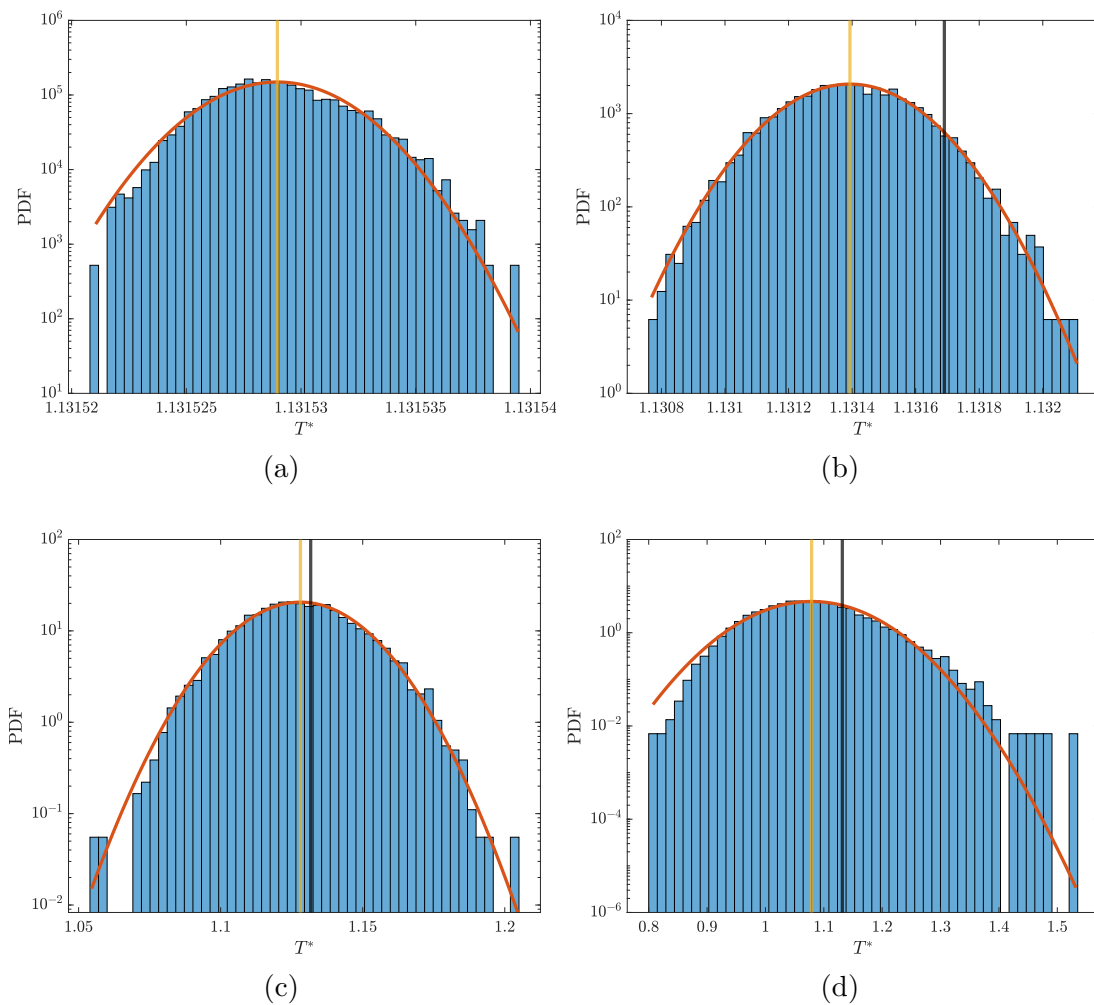
Figure 4.11: Histograms representing distributions of blow-up times in solutions of the stochastic problem (2.9) with different noise amplitudes (a) $\sigma = 10^{-6}$, (b) $\sigma = 10^{-4}$, (c) $\sigma = 10^{-2}$ and (d) $\sigma = 5 \times 10^{-2}$. Red lines represent the corresponding normal distribution (4.2). Yellow lines are the mean of the estimates for each case and black lines stands for the blow-up time in the deterministic case.
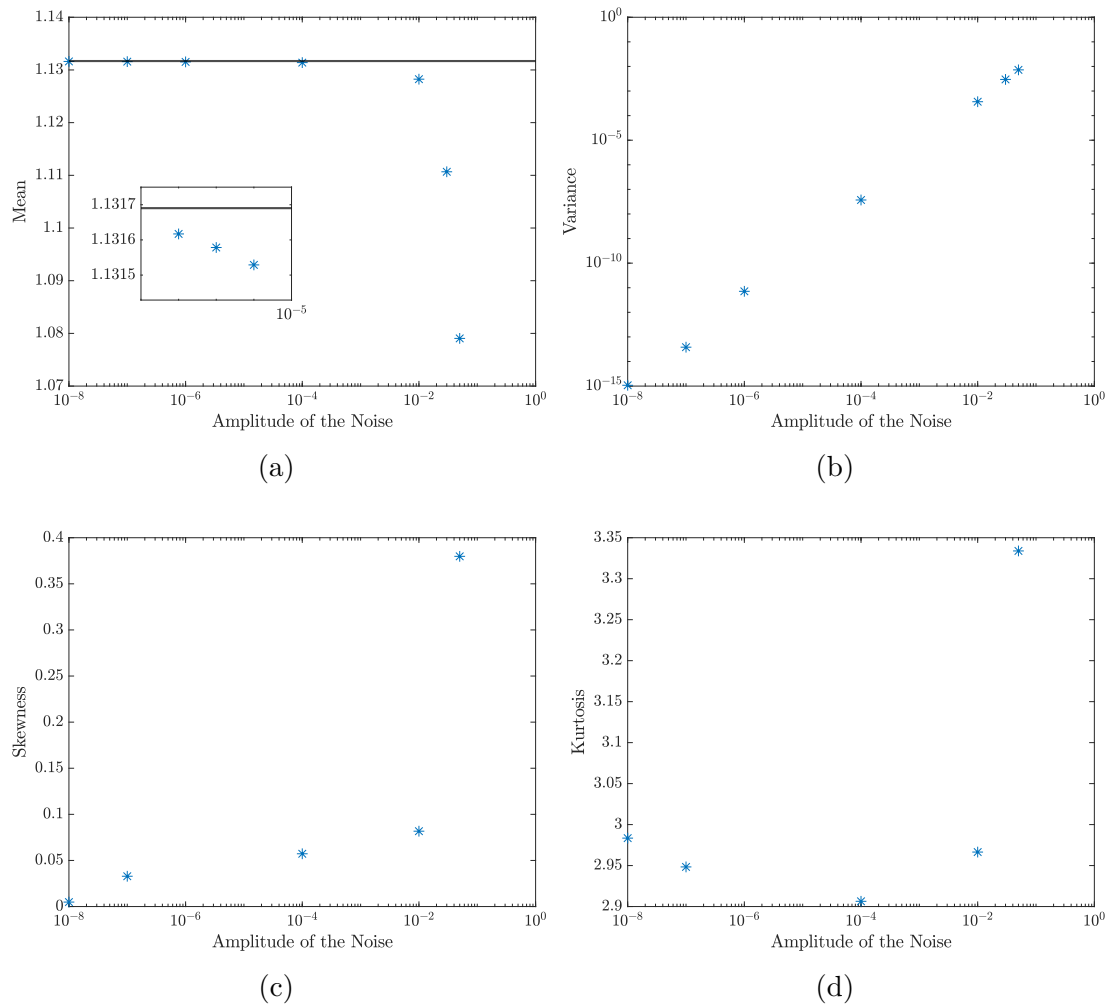
the third and fourth moments.

Figure 4.12: Mean (a) and variance (b) as a function of σ. The black line in (a) corresponds to the blow-up time of the determinsitic case. Skewness as a function of the amplitude of the noise σ (c). Kurtosis as a function of the amplitude of the noise σ (d).

Chapter 5

Summary and Conclusions

Regarding the deterministic case of the fractional Burgers equation, we worked with two quantities with important properties in either the supercritical and subcritical regimes, the enstrophy $\mathcal{E}(t)$ and the width of the analyticity strip $\delta(t)$. We studied their evolution in time as we vary the dissipation exponent α along the interval [0,1]. These quantities serve as indicator of the regularity of the solution and can be conveniently evaluated for a given numerical solution. Following Algorithm 3, we were able to use these two quantities to estimate when the blow-up time occurs. The first important result was to conclude that the blow-up time can be estimated by using any of theses quantities. Then, after choosing only to work with the enstrophy, we revealed a monotonous relation between the blow-up time T^* and the fractional dissipation exponent α (see figure 4.6a). An important aspect about this result was its consistency with some limiting cases, namely when $\nu \to 0$ and $\alpha \to 0$. We also have to highlight the fact that our numerical results exhibit evidence of blow-up in

H^1 when $\alpha \in [0, 1/4]$, which is outside the condition presented in Theorem 2.3. This supports the conjecture that that condition is not sharp.

For the stochastic case, we focused our study to only one value of the dissipation exponent α in the supercritical regime, $\alpha = 0.4$. The main goal was to analyze how additive noise affects the blow-up time estimates as compared to the deterministic case. The approach was through a Monte Carlo method. To sample the distribution of the blow-up times, we solved the system (2.9) using a colored-in-space Gaussian noise and a stochastic RK method for the integration in time. We found that, on average, the effect of the noise is to make the blow-up occurs earlier, which is opposite to the conjecture that noise smooths the solution. For small values of σ, it is expected that the blow-up time for the stochastic case coincides with the deterministic case. For the cases $\sigma \in [10^{-8}, 10^{-6}, 10^{-4}]$, our simulations showed that the difference between the estimates in the deterministic and the stochastic cases were $\mathcal{O}(10^{-3})$, which confirms what we were expecting.

Another interesting result was to find out that the estimates of the blow-up time for the system (2.9) are random variables normally distributed, for small values of σ. As the amplitude of the noise increases, the data becomes more asymmetrical and non-gaussian. The mean and the variance indicate a dependence on the size of the noise σ. If σ increases, the mean and the variance are decreasing and increasing, respectively. Although the change of the mean blow-up time with respect to the deterministic case does not appear very significant, its variance exhibit a substantial growth with the noise amplitude. Atypical values let us conclude that blow-up times that significantly deviate from the mean blow-up time show up more often as σ

increases.

Appendix A

Limiting Case $\alpha = 0$

Consider the equation

$$\partial_t u + \frac{1}{2} \partial_x u^2 + \nu\, u = 0 \quad \text{in } (0, T] \times (0, 2\pi), \tag{A.1a}$$

$$u(t, 0) = u(t, 2\pi) \quad \text{for } t \in (0, T], \tag{A.1b}$$

$$u(0, x) = g(x) \quad \text{for } x \in (0, 2\pi), \tag{A.1c}$$

where $\nu > 0$, $T > 0$ denotes the length of the time window and $g(x) \in C^\infty(0, 2\pi)$. Applying the method of characteristics we get

$$\frac{dt}{ds} = 1, \quad t(0) = 0, \tag{A.2}$$

$$\frac{dx}{ds} = u, \quad x(0) = x_0, \tag{A.3}$$

$$\frac{du}{ds} = -\nu u, \quad u(0) = u(0, x_0) = g(x_0). \tag{A.4}$$

Solving equations (A.2) and (A.4), we obtain

$$t(s) = s \quad \text{and} \quad u(s) = g(x_0)e^{-\nu s}. \tag{A.5}$$

Therefore, the equation for the characteristics is

$$x(t) = \left(x_0 + \frac{g(x_0)}{\nu} \right) - \frac{g(x_0)}{\nu}e^{-\nu t}. \tag{A.6}$$

If we are capable of expressing x_0 as a function of x and t, then a solution of system (A.1) would be

$$u(t, x(t)) = g(x_0(x(t)))e^{-\nu t}, \quad \text{for} \quad t \in [0, T^*]. \tag{A.7}$$

Let us identify T^*. First, if the characteristic curves never intercept each other, then $T^* = \infty$. Second, assume that the characteristic lines cross each other and suppose that it first happens at a point (T^*, x_*). So

$$\frac{\partial u}{\partial x}(t, x_*) \to \infty, \quad \text{as} \quad t \to T^*,$$

and $u(t, x)$ stops being a classical solution. Now,

$$
\begin{aligned}
\frac{\partial u}{\partial x} &= \frac{\partial}{\partial x} g(x_0)e^{-\nu t} \\
&= g'(x_0)e^{-\nu t}\frac{\partial x_0}{\partial x} \\
&= \frac{g'(x_0)e^{-\nu t}}{1 + \frac{1}{\nu}g'(x_0) - \frac{1}{\nu}g'(x_0)e^{-\nu t}},
\end{aligned}
$$

where the last equality follows from the implicit derivative $\frac{\partial x_0}{\partial x}$ in expression (A.6).

Since $t > 0$, $\nu > 0$, and $g(x) \in C^\infty(0, 2\pi)$, then

$$\frac{\partial u}{\partial x}(t, x_*) \to \infty \quad \text{implies that} \quad 1 + \frac{1}{\nu}g'(x_0) - \frac{1}{\nu}g'(x_0)e^{-\nu t} = 0.$$

Therefore

$$t = -\frac{1}{\nu}\ln\left(\frac{\nu}{g'(x_0)} + 1\right), \quad \text{as long as} \quad g'(x_0) + \nu < 0. \tag{A.8}$$

In other words, if $x_*(0) = x_0$ and $g'(x_0) + \nu < 0$, then the solution along the characteristic starting at $(0, x_0)$ fails to be smooth at the time given in (A.8). So considering the smallest time where it can happen, we will get the blow-up time. Hence,

$$T^* = \inf_{x_0 \in (0, 2\pi)}\left\{-\frac{1}{\nu}\ln\left(\frac{\nu}{g'(x_0)} + 1\right)\right\} = -\frac{1}{\nu}\ln\left(\frac{\nu}{\inf_{x_0 \in (0, 2\pi)} g'(x_0)} + 1\right). \tag{A.9}$$

Thus, we have found that the blow-up time for the equation (A.1) is

$$T^* = \begin{cases} \infty & \text{if } g'(x) + \nu \geq 0 \text{ for all } x \in [0, 2\pi], \\ -\frac{1}{\nu}\ln\left(\frac{\nu}{\inf g'(x)} + 1\right) & \text{otherwise.} \end{cases} \tag{A.10}$$

To characterize the form of the solution to the problem, we need to ensure that x_0 can be explicitly written as a function of $x(t)$ and t. Let

$$F(x, t, b) = x - \left(b + \frac{g(b)}{\nu}\right) + \frac{g(b)}{\nu}e^{-\nu t}, \quad \epsilon < t < T^*, \ x, \ b \in (0, 2\pi),$$

where ϵ is a positive number. Notice that $F(x, t, b)$ is differentiable at any point (t, x, x_0) in its domain and $F(x, t, x_0) = 0$. Also,

$$\partial_b F(x, t, x_0) = -\frac{g'(x_0)}{\nu} + \frac{g'(x_0)}{\nu} e^{-\nu t} \neq 0 \quad \text{for} \quad \epsilon < t < T^*.$$

Therefore, exist a unique smooth function $x_0 = x_0(t, x(t))$ over an open neighbourhood of (t, x) such that $F(t, x, x_0(t, x(t))) = 0$ by the implicit function theorem.

Appendix B

Structure of the Stochastic Forcing of System (2.9)

In this appendix we will show why considering a white noise in system (2.9) is not a good choice for our purposes. A white noise is defined as a Wiener process with $\gamma_j = 1$ for all $j \in \mathbb{N}$ in (2.11). Instead, we must consider the coefficients in expression (2.11) as in (2.12). To begin with, let us consider the mild solution (2.14) of system (2.9). Now, we are going to study each term of the right-hand side of equation (2.14). The following arguments were adapted to the fractional case from the analysis made in [PP18].

First term: Suppose $g \in L_p^2(0, 2\pi)$, so

$$\|g\|_{L_p^2}^2 = \frac{1}{2\pi} \int_0^{2\pi} |g(x)|^2 dx = \sum_{k \in \mathbb{Z}} |\widehat{g}_k|^2 < \infty,$$

where $\{\widehat{g}_k\}_{k\in\mathbb{Z}}$ are the Fourier coefficients of g. Since we can write g as

$$g(x) = \sum_{k\in\mathbb{Z}} \widehat{g}_k e^{ikx},$$

note that

$$e^{-tA}g = e^{-tA}\sum_{k\in\mathbb{Z}}\widehat{g}_k e^{ikx} = \sum_{k\in\mathbb{Z}}\widehat{g}_k e^{-tA}e^{ikx} = \sum_{k\in\mathbb{Z}}\widehat{g}_k e^{-\nu t|k|^{2\alpha}}e^{ikx}.$$

Therefore

$$\left\|e^{tA}g\right\|_{H_p^1}^2 = \left\|\sum_{k\in\mathbb{Z}}\widehat{g}_k e^{-\nu t|k|^{2\alpha}}e^{ikx}\right\|_{H_p^1}^2$$

$$= \left\|\sum_{k\in\mathbb{Z}}\widehat{g}_k e^{-\nu t|k|^{2\alpha}}e^{ikx}\right\|_{L_p^2}^2 + \left\|\sum_{k\in\mathbb{Z}}\widehat{g}_k ik\, e^{-\nu t|k|^{2\alpha}}e^{ikx}\right\|_{L_p^2}^2$$

$$= \sum_{k\in\mathbb{Z}}\left|e^{-2\nu t|k|^{2\alpha}}\right||\widehat{g}_k|^2 + \sum_{k\in\mathbb{Z}}k^2\left|e^{-2\nu t|k|^{2\alpha}}\right||\widehat{g}_k|^2$$

$$= \sum_{k\in\mathbb{Z}}(1+k^2)\left|e^{-2\nu t|k|^{2\alpha}}\right||\widehat{g}_k|^2$$

$$= \sum_{k\in\mathbb{Z}}(1+k^2)e^{-2\nu t|k|^{2\alpha}}|\widehat{g}_k|^2.$$

Since

$$\sum_{k\in\mathbb{Z}}|\widehat{g}_k|^2 < \infty, \quad \text{and} \quad \lim_{k\to\pm\infty}(1+k^2)e^{-2\nu t|k|^{2\alpha}} = 0,$$

then $\left\|e^{tA}g\right\|_{H_p^1}^2 < \infty$ by Abel's test.

Second term: Let us assume that $u \in L^2\left(\Omega, C\left([0,T], L_p^4\right)\right)$, so that $u^2 \in$

$L^2\left(\Omega, C\left([0,T], L_p^2\right)\right)$. There exist $\widehat{y}_k$'s such that

$$u^2 = \sum_{k\in\mathbb{Z}} \widehat{y}_k \phi_k, \quad \text{with} \quad \sum_{k\in\mathbb{Z}} \|\widehat{y}_k\|^2_{L^2(\Omega, C([0,T],\mathbb{C}))} = \sum_{k\in\mathbb{Z}} \mathbb{E}\left[\sup_{0\le t\le T} |\widehat{y}_k|^2\right] < \infty.$$

Then

$$\partial_x u^2 = i \sum_{k\in\mathbb{Z}} k\, \widehat{y}_k \phi_k,$$

and

$$\int_0^t \frac{1}{2} e^{-(t-s)A} \partial_x u^2 ds = \int_0^t \frac{1}{2} e^{-(t-s)A} \left(i \sum_{k\in\mathbb{Z}} k\, \widehat{y}_k(s)\phi_k\right) ds$$

$$= \sum_{k\in\mathbb{Z}} \left[\int_0^t \frac{ik}{2} \widehat{y}_k(s) e^{-(t-s)A} \phi_k ds\right]$$

$$= \sum_{k\in\mathbb{Z}} \left[\int_0^t \frac{ik}{2} \widehat{y}_k(s) e^{-(t-s)A} e^{ikx} ds\right]$$

$$= \sum_{k\in\mathbb{Z}} \left[\int_0^t \frac{ik}{2} \widehat{y}_k(s) e^{-\nu(t-s)|k|^{2\alpha}} e^{ikx} ds\right]$$

$$= \sum_{k\in\mathbb{Z}} \left[\int_0^t \frac{ik}{2} \widehat{y}_k(s) e^{-\nu(t-s)|k|^{2\alpha}} ds\right] \phi_k.$$

Note that

$$\left| \int_0^t \frac{ik}{2} \widehat{y}_k(s) e^{-\nu(t-s)|k|^{2\alpha}} ds \, \phi_k \right| = \left| \int_0^t \frac{ik}{2} \hat{y}_k(s) e^{-\nu(t-s)|k|^{2\alpha}} ds \right|$$

$$\leq \int_0^t \left| \frac{ik}{2} \widehat{y}_k(s) e^{-\nu(t-s)|k|^{2\alpha}} \right| ds$$

$$= \int_0^t \frac{|k|}{2} \left| e^{-\nu(t-s)|k|^{2\alpha}} \right| |\widehat{y}_k(s)| \, ds$$

$$\leq \frac{|k|}{2} \int_0^t e^{-\nu(t-s)|k|^{2\alpha}} ds \sup_{0 \leq t \leq T} |\widehat{y}_k(t)|$$

$$= \left(\frac{1 - e^{-\nu t |k|^{2\alpha}}}{2\nu |k|^{2\alpha - 1}} \right) \sup_{0 \leq t \leq T} |\widehat{y}_k(t)|$$

$$= \frac{1}{2\nu |k|^{2\alpha - 1}} \sup_{0 \leq t \leq T} |\widehat{y}_k(t)| \,,$$

so

$$\left\| \int_0^t \frac{1}{2} e^{(t-s)A} \partial_x u^2 ds \right\|_{L^2(\Omega, H_p^1)}^2 \leq \left\| \sum_{k \in \mathbb{Z}} \frac{1}{2\nu |k|^{2\alpha-1}} \sup_{0 \leq t \leq T} |\widehat{y}_k(t)| \right\|_{L^2(\Omega, H_p^1)}^2$$

$$\leq \sum_{k \in \mathbb{Z}} \left\| \frac{1}{2\nu |k|^{2\alpha-1}} \sup_{0 \leq t \leq T} |\widehat{y}_k(t)| \right\|_{L^2(\Omega, \mathbb{C})}^2$$

$$= \sum_{k \in \mathbb{Z}} \frac{1}{4\nu^2 |k|^{4\alpha-2}} \left\| \sup_{0 \leq t \leq T} |\widehat{y}_k(t)| \right\|_{L^2(\Omega, \mathbb{C})}^2$$

$$= \sum_{k \in \mathbb{Z}} \frac{1}{4\nu^2 |k|^{4\alpha-2}} \| \widehat{y}_k \|_{L^2(\Omega, C([0,T], \mathbb{C}))}^2$$

since

$$\lim_{k \to \pm\infty} \frac{1}{4\nu^2 |k|^{4\alpha-2}} = 0, \quad \text{for } 1/2 \leq \alpha \leq 1 \quad \text{and} \quad \sum_{k \in \mathbb{Z}} \| \widehat{y}_k \|_{L^2(\Omega, C([0,T], \mathbb{C}))}^2 < \infty,$$

they imply that if $1/2 \leq \alpha \leq 1$, the second term is also in H_p^1 by Abel's test.

Third term: We can write this term as a Fourier series

$$\sigma \int_0^t e^{-(t-s)A} dW(s) = \sum_{k \in \mathbb{Z}} \widehat{W}_k(t) \phi_k,$$

where $\widehat{W}_k$ can be computed as

$$\widehat{W}_k = \left\langle \sigma \int_0^t e^{-(t-s)A} dW(s), \phi_k \right\rangle,$$

and $\langle \cdot, \cdot \rangle$ is the inner product on $L_p^2(0, 2\pi)$ given by

$$\langle u, v \rangle = \frac{1}{2\pi} \int_0^{2\pi} u\bar{v} \, dx,$$

for some u, $v \in L_p^2(0, 2\pi)$.

Considering $k > 0$ (cases $k < 0$ or $k = 0$ are analogous), we get

$$\widehat{W}_k = \frac{1}{2\pi} \int_0^{2\pi} \left(\sigma \int_0^t e^{-(t-s)A} dW(s) \right) \phi_k dx$$

$$= \frac{\sigma}{2\pi} \int_0^{2\pi} \left(\int_0^t e^{-(t-s)A} \left[\sum_{j=1}^\infty \sqrt{2} \cos(j\,x)\, d\beta_{2j}(s) + \sum_{j=1}^\infty \sqrt{2} \sin(j\,x)\, d\beta_{2j-1}(s) \right] \right) \phi_k dx$$

$$= \frac{\sigma}{2\pi} \int_0^{2\pi} \int_0^t e^{-(t-s)A} \phi_k \left[\sum_{j=1}^\infty \sqrt{2} \cos(j\,x)\, d\beta_{2j}(s) + \sum_{j=1}^\infty \sqrt{2} \sin(j\,x)\, d\beta_{2j-1}(s) \right] dx$$

$$= \frac{\sigma}{2\pi} \int_0^{2\pi} \int_0^t e^{-\nu(t-s)k^{2\alpha}} \phi_k \left[\sum_{j=1}^\infty \sqrt{2} \cos(j\,x)\, d\beta_{2j}(s) + \sum_{j=1}^\infty \sqrt{2} \sin(j\,x)\, d\beta_{2j-1}(s) \right] dx$$

$$= \sigma \int_0^t e^{-\nu(t-s)k^{2\alpha}} \sum_{j=1}^\infty \sqrt{2} \left(\frac{1}{2\pi} \int_0^{2\pi} \cos(j\,x) \phi_k dx \right) d\beta_{2j}(s) dx$$

$$+ \sigma \int_0^t e^{-\nu(t-s)k^{2\alpha}} \sum_{j=1}^\infty \sqrt{2}\,(s) \left(\frac{1}{2\pi} \int_0^{2\pi} \sin(j\,x) \phi_k dx \right) d\beta_{2j-1}$$

$$= \sigma \int_0^t e^{-\nu(t-s)k^{2\alpha}} \left[\sum_{j=1}^\infty \sqrt{2} \langle \cos(jx), \phi_k \rangle\, d\beta_{2j}(s) + \sum_{j=1}^\infty \sqrt{2} \langle \sin(jx), \phi_k \rangle\, d\beta_{2j-1}(s) \right]$$

$$= \sigma \int_0^t e^{-\nu(t-s)k^{2\alpha}} \left[\frac{\sqrt{2}}{2}\, d\beta_{2k}(s) - \frac{\sqrt{2}}{2} i\, d\beta_{2k-1}(s) \right].$$

Using the Itô isometry [LPS14], we obtain

$$\left\| \widehat{W}_k(t) \right\|_{L^2(\Omega,\mathbb{C})}^2 = \mathbb{E}\left[\left| \widehat{W}_k(t) \right|^2 \right] = \mathbb{E}\left[\left| \int_0^t \sigma e^{-\nu(t-s)|k|^{2\alpha}} \left[\frac{\sqrt{2}}{2}\, d\beta_{2k}(s) - \frac{\sqrt{2}}{2} i\, d\beta_{2k-1}(s) \right] \right|^2 \right]$$

$$= \int_0^t \mathbb{E}\left[\sigma^2 e^{-2\nu(t-s)|k|^{2\alpha}} \left| \frac{\sqrt{2}}{2} - i\frac{\sqrt{2}}{2} \right|^2 \right] ds$$

$$= \int_0^t \sigma^2 e^{-2\nu(t-s)|k|^{2\alpha}} ds$$

$$= \frac{\sigma^2}{2\nu|k|^{2\alpha}} \left(1 - e^{-2\nu t |k|^{2\alpha}} \right),$$

then $\left\|\widehat{W}_k(t)\right\|^2_{L^2(\Omega,\mathbb{C})} < \infty$ for each k. Therefore

$$\left\|\sigma \int_0^t e^{-(t-s)A}dW(s)\right\|^2_{L^2(\Omega,L_p^2)} = \sum_{k\in\mathbb{Z}} \left\|\widehat{W}_k\right\|^2_{L^2(\Omega,\mathbb{C})}$$

$$= \sum_{k\in\mathbb{Z}^-} \left\|\widehat{W}_k\right\|^2_{L^2(\Omega,\mathbb{C})} + \left\|\widehat{W}_0\right\|^2_{L^2(\Omega,\mathbb{C})} + \sum_{k\in\mathbb{Z}^+} \left\|\widehat{W}_k\right\|^2_{L^2(\Omega,\mathbb{C})}$$

is bounded because each term term of the sum is bounded. In conclusion, the third term is in L^2. Now, let us check if it belongs to H_p^1.

$$\left\|\sigma \int_0^t e^{(t-s)A}dW(s)\right\|^2_{L^2(\Omega,H_p^1)} = \sum_{k\in\mathbb{Z}}(1+k^2)\left\|\widehat{W}_k\right\|^2_{L^2(\Omega,\mathbb{C})} = \sum_{k\in\mathbb{Z}}\frac{\sigma^2(1+k^2)}{2\nu|k|^{2\alpha}}\left(1 - e^{-2\nu t|k|^{2\alpha}}\right),$$

which is a divergent series. Hence, it is not possible to guarantee that the mild solution (2.14) from system (2.9) is well defined in H_p^1 by considering white noise.

To ensure the third term of the mild solution (2.14) in H_p^1, a representation of the noise with ℓ^2 summable coefficients is considered. We follow the choice made in [PP18] for $\{\gamma_j\}_{j\in\mathbb{N}}$ as $\gamma_0 = 0$, $\gamma_{2k-1} = \gamma_{2k} = \frac{1}{k}$, $k > 0$. With this, the analysis for the third term is

$$\widehat{W}_k = \sigma \int_0^t e^{-\nu(t-s)k^{2\alpha}}\left[\frac{\sqrt{2}}{2k}\,d\beta_{2k}(s) - \frac{\sqrt{2}}{2k}i\,d\beta_{2k-1}(s)\right],$$

and

$$\left\|\widehat{W}_k(t)\right\|^2_{L^2(\Omega,\mathbb{C})} = \frac{\sigma^2}{2\nu|k|^{2\alpha+2}}\left(1 - e^{-2\nu t|k|^{2\alpha}}\right).$$

So

$$\left\| \sigma \int_0^t e^{-(t-s)A} dW(s) \right\|_{L^2(\Omega, H_p^1)}^2 = \sum_{k \in \mathbb{Z}} \frac{\sigma^2(1+k^2)}{2\nu |k|^{2\alpha+2}} \left(1 - e^{-2\nu t |k|^{2\alpha}} \right),$$

which is a convergent series as long as $\alpha > 1/2$. Also,

$$\|W(t)\|_{L^2(\Omega, L^2)}^2 = \sum_{j \in \mathbb{N}} |\gamma_j|^2 \, \|\beta_j(t)\|_{L^2(\Omega, \mathbb{C})}^2 \, \|\chi_j\|_{L^2}^2 = t \sum_{j \in \mathbb{N}} \gamma_j^2 = \frac{\pi^2}{3} t.$$

which means that the noise $W(t)$ is square-integrable in L^2 for all times. Under this choice, the enstrophy is a well defined quantity when $\alpha > 1/2$. So, in our simulations we will be using the the noise with these γ_j coefficients. Noise of this type is referred as *colored-in-space Gaussian noise.*

References

[AP11]   D. Ayala and B. Protas, *On Maximum Enstrophy Growth in a Hydrodynamic System*, Physica D: Nonlinear Phenomena **240** (2011), 1553-1563.

[AP14]   _____ , *Vortices, Maximum Growth and the Problem of Finite-Time Singularity Formation*, Fluid Dynamics Research **46** (2014), 031404.

[Aya10]   D. Ayala, *Maximum enstrophy growth in Burgers equation*, Master thesis, McMaster University (2010).

[Aya14]   _____ , *Extreme vortex states and singularity formation in incompressible flows*, PhD thesis, McMaster University (2014).

[BB12]   M. Bustamante and M. Brachet, *Interplay between the Beale-Kato-Majda Theorem and the Analyticity-Strip Method to Investigate Numerically the Incompressible Euler Singularity Problem*, Physical Review **86** (2012), 066302.

[Bew09]   T. Bewley, *Numerical Renaissance*, Renaissance Press, 2009.

[BK08]   M. Bustamante and R. Kerr, *3D Euler about a 2D Symmetry Plane*, Physica D **237** (2008), 1912-1920.

[Cha87]   C. Chang, *Numerical Solution of Stochastic Differential Equations with Constant Diffusion Coefficients*, Mathematics of Computation **49** (1987), no. 180, 523-542.

[DDFR12]   R. Dalang, M. Dozzi, F. Flandoli, and F. Russo, *Stochastic Analysis: A Series of Lectures*, Vol. 68, Birkhäuser, 2012.

[Doe09] C. Doering, *The 3D Navier-Stokes Problem*, Annual Reviews **41** (2009), 109-128.

[Fef00] L. Fefferman, *Existence and smoothness of the Navier-Stokes equation* (2000), `https://www.claymath.org/sites/default/files/navierstokes.pdf`.

[Fla15] F. Flandoli, *Random Perturbation of PDEs and Fluid Dynamic Models*, Springer, 2015.

[FT89] C. Foias and R. Temam, *Gevrey Class Regularity for the Solutions of the Navier-Stokes Equations*, J. Funct. Anal. **87** (1989), 359-369.

[KL04] H. Kreiss and J. Lorenz, *Initial-Boundary Value Problems and the Navier-Stokes Equations*, Vol. 47, SIAM, 2004.

[KNS08] A. Kiselev, F. Nazarov, and R. Shterenberg, *Blow up and Regularity for Fractal Burgers Equation*, Dyn. Partial. Differ. Equ. **5** (2008), 211-240.

[KP02] N. Katz and N. Pavlović, *A Cheap Caffarelli-Kohn-Nirenberg Inequality for the Navier-Stokes Equation with Hyper-Dissipation*, GAFA, Geometric And Functional Analysis **12** (2002), 355-379.

[LPS14] G. Lord, C. Powell, and T. Shardlow, *An Introduction to Computational Stochastic PDEs*, CAMBRIDGE, 2014.

[Pel12] D. Pelinovsky, *Sharp Bounds on Enstrophy Growth in the Viscous Burgers Equation*, Proc. R. Soc. A **468** (2012a), 3636-3648.

[Pey02] R. Peyret, *Spectral Methods for Incompressible Viscous Flow*, Vol. 148 of Applied Mathematical Sciences, Springer, 2002.

[PP18] D. Poças and B. Protas, *Transient Growth in Stochastic Burgers Flow*, Discrete and Continuous Dynamical Systems **23** (2018), 2371-2391.

[SSF83] C. Sulem, P. Sulem, and H. Frisch, *Tracing complex singularities with spectral methods*, Journal of computational physics **50** (1983), 138-161.

[Tre00] L. Trefethen, *Spectral Methods in MATLAB*, SIAM, 2000.

[YP18] D. Yun and B. Protas, *Maximum Rate of Growth of Enstrophy in Solutions of the Fractional Burgers Equation*, Journal of Nonlinear Science **28** (2018), 395-422.